



# Contrasting sea-surface responses between the western Mediterranean Sea and eastern subtropical latitudes of the North Atlantic during abrupt climatic events of MIS 3

Aurélie Pénaud, Frédérique Eynaud, María-Fernanda Sánchez-Goñi, B. Malaize, Jean-Louis Turon, L. Rossignol

## ► To cite this version:

Aurélie Pénaud, Frédérique Eynaud, María-Fernanda Sánchez-Goñi, B. Malaize, Jean-Louis Turon, et al.. Contrasting sea-surface responses between the western Mediterranean Sea and eastern subtropical latitudes of the North Atlantic during abrupt climatic events of MIS 3. *Marine Micropaleontology*, 2011, 80, pp.1-17. 10.1016/j.marmicro.2011.03.002 . insu-00588836

**HAL Id: insu-00588836**

**<https://hal-insu.archives-ouvertes.fr/insu-00588836>**

Submitted on 26 Apr 2011

**HAL** is a multi-disciplinary open access archive for the deposit and dissemination of scientific research documents, whether they are published or not. The documents may come from teaching and research institutions in France or abroad, or from public or private research centers.

L'archive ouverte pluridisciplinaire **HAL**, est destinée au dépôt et à la diffusion de documents scientifiques de niveau recherche, publiés ou non, émanant des établissements d'enseignement et de recherche français ou étrangers, des laboratoires publics ou privés.

**Contrasting sea-surface responses between the western Mediterranean Sea and eastern  
subtropical latitudes of the North Atlantic during abrupt climatic events of MIS 3**

**Penaud A.<sup>(a,b)</sup>\*, Eynaud F.<sup>(b)</sup>, Sánchez-Goñi M.<sup>(c)</sup>, Malaizé B.<sup>(b)</sup>,  
Turon J.L.<sup>(b)</sup>, Rossignol L.<sup>(b)</sup>**

*(a) UMR 6538 Domaines Océaniques, IUEM-UBO, F-29280 Plouzané, France*

*(b) UMR 5805 EPOC, Université de Bordeaux 1, F-33405 Talence, France*

*(c) EPHE, UMR 5805 EPOC, Talence, F-33405 Talence, France*

\*Corresponding author. Tel.: +33-298-498-741; fax: +33-298-498-760.

*E-mail address:* aurelie.penaud@univ-brest.fr.

**ABSTRACT**

Dinoflagellate cyst (dinocyst) analysis was conducted on two cores from the SW Iberian margin and central Alboran Sea from which high quality records of Marine Isotope Stage 3 have been previously derived. Our aim in this study is to compare the dinocyst signature between 50 and 25 ka BP with existing datasets of foraminiferal and geochemical proxies related to hydrological parameters. Quantitative reconstructions of sea-surface temperatures (SSTs) and salinities (SSS) based on dinocysts are performed for the first time in this area. The results are compared to SSTs derived from planktonic foraminifera and alkenone measurements, and to SSS calculated from planktonic  $\delta^{18}\text{O}$  and foraminiferal SST. Significant oscillations related to Dansgaard-Oeschger cycles are recorded in both cores. Dinocyst-derived hydrological parameters exhibit synchronous fluctuations and similar values to those derived from the other methods, in particular when considering quantitative reconstructions for February based on foraminifera and dinocysts. Our study shows that the influence of subpolar waters was felt during each Greenland Stadial (GS) off Portugal, and that the amplification of the Heinrich Stadial cooling in the Alboran Sea was related to the penetration of subpolar waters through the Strait of Gibraltar. During Greenland Interstadials (GI), we provide evidence for the occurrence of warm and nutrient-rich sea-surface waters in the Alboran Sea, probably due to gyre-induced upwelling. Finally, the difference between August and February dinocyst SST estimates suggests higher seasonal contrasts during GS compared to GI at the two core sites. Additionally, precession appears to have an imprint on dinocyst-derived long-term seasonality record. However, this observation needs to be confirmed by longer records.

**KEYWORDS:** *Dinocysts; SST and SSS quantification; Dansgaard-Oeschger; Greenland and Heinrich stadials; Alboran Sea; Iberian margin.*

## 1. Introduction

The climate of the last glacial was characterised by a distinctive oscillatory mode, the so-called Dansgaard-Oeschger (D-O) cycles, originally described and defined in Greenland ice cores (Johnsen et al., 1992; Dansgaard et al., 1993; Grootes et al., 1993) and paced by an empirical 1470-year factor, the nature of which being presently not known (Schulz et al., 1999; Moreno et al., 2005; Voelker et al., 2006). Greenland Interstadials (GI) and Greenland Stadials (GS) including Heinrich Stadials (HS, following Sánchez-Goñi and Harrison, 2010), have previously been observed in marine climate records worldwide (e.g. Voelker et al., 2002; Hemming, 2004; Clement and Peterson, 2008). The impacts of HS, which primarily correspond to large ice-sheet collapses, are now fairly well characterised in the NE Atlantic and Mediterranean areas. Their occurrence is associated with enhanced aridity in the adjacent borderlands (Combourieu-Nebout et al., 2002; Sánchez-Goñi et al., 2002), increases in northward Saharan dust transport (Moreno et al., 2002; Bout-Roumazielles et al., 2007) and sea-surface temperature coolings in the western Mediterranean Sea (e.g. Cacho et al., 1999) and on the Portuguese margin (e.g. Cayre et al., 1999; Pailler and Bard, 2002; de Abreu et al., 2003). However, the forcing mechanisms behind the initiation of HS and the inferred reorganisation of Meridional Overturning Circulation within the last glacial period are still a matter of debate (Kageyama et al., 2009). Furthermore, a full understanding of this rapid transmission of millennial-scale climatic variability from boreal to subtropical latitudes, involving both atmospheric and oceanic processes, remains elusive. It has been demonstrated that convection in the western Mediterranean, and thus export of Mediterranean Outflow Water (MOW), was strengthened during GS of the last 50 ka (Cacho et al., 2000, 2006; Sierro et al., 2005; Voelker et al., 2006; Toucanne et al., 2007; Frigola et al., 2008). Consequently, it has been suggested that the Mediterranean could act as a major trigger for

the Meridional Overturning Circulation to switch from stadial to interstadial mode through the influence of MOW, providing saline water to the North Atlantic at times when the Meridional Overturning Circulation was partially interrupted (Johnson, 1997; Bigg and Wadley, 2001; Rogerson et al., 2006; Voelker et al., 2006). The production of MOW is mainly controlled by the salinity budget of the Mediterranean Sea which depends on the climate characteristics over the region and therefore on dominant modes of climatic variability, notably the North Atlantic Oscillation (NAO). At present, the NAO pattern, oscillating at decadal and centennial scales, has a strong influence on climate over a large part of Europe during winter, by affecting the storm tracks and the associated relative moisture over the Mediterranean and northern Europe (e.g. Hurrell, 1995; Serreze et al., 1997; Osborn et al., 1999). Over the eastern Atlantic subtropical sector, it has been argued that this oscillation also has an imprint at centennial or millennial timescales, and has been implicated in abrupt climatic events of the last glacial (Sánchez-Goñi et al., 2002; Moreno et al., 2005; Bout-Roumazeilles et al. 2007; Danialu et al., 2007; Naughton et al., 2009). Consequently, a change between two periods, each of them characterised by sustained frequencies of a particular atmospheric configuration over several centuries, may have caused significant variations of hydrological exchanges through time between the Atlantic and the Mediterranean Sea (Moreno et al., 2005).

Previous high resolution palynological analysis of dinoflagellate cysts (dinocysts) and pollen on core MD95-2042, collected off Portugal, indicate abrupt changes in sea surface and atmospheric conditions, respectively, in response to D-O cycles (Eynaud, 1999; Sánchez-Goñi et al., 2000). Additionally, a climatic contrast has been observed with respect to precipitation between the SW Iberian margin and the Alboran region, with dryer conditions in southeastern Iberia than in its southwestern part (Sánchez-Goñi et al., 2002). However, these studies do not quantify either changes in SST and SSS, or discuss the possible impact of the observed precipitation gradient on

87 the hydrological conditions of both sides of the Strait of Gibraltar between 25 and 50 ka BP. To  
88 fill this gap, we have analyzed dinocyst assemblages from core MD95-2043, located in the  
89 Alboran Sea, and applied transfer functions. Furthermore, we have tested, for subtropical  
90 latitudes, the robustness of quantitative paleotemperature and paleosalinity reconstructions  
91 inferred from dinocysts against other proxy reconstructions (i.e. dinocyst- *versus* foraminifera-  
92 *versus* alkenone- derived SST, and dinocyst- derived SSS *versus* SSS estimates calculated on the  
93 basis of the  $\delta^{18}\text{O}$  of *Globigerina bulloides* associated with foraminiferal SST).

## 2. Core locations and present-day environmental settings

Calypso cores MD95-2043 (36°8.6'N; 2°37.3'W; 1841 m water depth; 36 m long) and MD95-2042 (37°48'N; 10°10'W; 3146 m water depth; 39.56 m long) were retrieved from the central Alboran Sea and the SW Iberian margin, respectively (Fig. 1), and were both collected by the oceanographic R/V Marion Dufresne during the 1995 International Marine Global Change Studies I (IMAGES I) cruise (Bassinot and Labeyrie, 1996).

The Mediterranean Sea is located between the path of the mid-latitude westerlies which dominate northern and central Europe, and the Azores High. At present, this basin experiences a typical seasonal cycle marked by cool-wet winters, and warm-dry summers. The resulting Mediterranean water budget is marked by a strong freshwater deficit due to a net excess evaporation (Béthoux, 1979, 1984). During winter and spring, intense cold and dry continental air outbursts induce strong evaporation and cooling in the northern Mediterranean Sea, and thus an increased density of surface water masses. As a result, surface waters sink in several specific Mediterranean regions, flow westward, and finally form the Mediterranean Outflow Water (MOW). The outflow current is exported at depth towards the Atlantic Ocean, through the narrow Strait of Gibraltar (main sill depth of 280 m) and is split into two stability levels: an upper core centred between 500 m and 800 m, and a more saline and dense lower core found between 1000 and 1400 m (Ambar et al., 2002). The MOW can be traced in the North Atlantic as a salinity and temperature maximum at about 1 km depth (e.g. Hill and Mitchelson-Jacob, 1993; Iorga and Lorzier, 1999; O'Neill-Baringer and Price, 1999), and mixes progressively with North Atlantic Intermediate Waters (NAIW; Mauritzen, 1996). In the opposite direction, a North-Atlantic low-salinity surface current penetrates the Alboran Sea and mixes with Levantine Intermediate Waters (which resurface in the westernmost part of the Alboran Sea), forming the so-called Modified Atlantic

Waters (MAW). The strong flow of MAW along the coast of Spain initiates the formation of two anticyclonic gyres, the Western and Eastern Alboran Gyres (WAG and EAG; Fig. 1) whose position and intensity fluctuate at a seasonal scale. The degree of development of the EAG, under which core MD95-2043 is located (Fig. 1), controls the position and intensity of the permanent Almeria-Oran Front (AOF; Fig. 1) (Tintoré et al., 1988; Rohling et al., 1995, 2009; Viúdez and Tintoré, 1995). Upwelling cells occur along the AOF, this front marking the deflection of MAW along the Algerian margin, forming the Algerian Current (AC; Fig. 1).

The main modern hydrological structures and currents of the western Iberian margin form part of the North Atlantic Eastern Boundary Current (Fig. 1; Peliz et al., 2005; Relvas et al., 2007). They are driven by the North Atlantic subtropical gyre intensity in relation to the seasonal displacement of the Azores High (e.g. Fiúza, 1984; Fiúza et al., 1998). Core MD95-2042 is located in the seasonal coastal upwelling band of the Portugal-Canary eastern boundary upwelling system that is active mainly from April to October (Aristegui et al., 2005; Peliz et al., 2005). The upwelling predominantly receives North Atlantic Central Waters (NACW) and, in part, also MOW (Sánchez and Relvas, 2003). Occasionally, during winter months, a warm northward-flowing surface current known as the Iberian Poleward Current or Portugal Coastal Counter Current is formed by coastal convergence along the western Iberian margin. This phenomenon occurs when weak northerlies are interspersed with strong south-southwesterly winds (e.g. Fiúza et al., 1998; Peliz et al., 2005). This current can be traced as far as the Bay of Biscay where it is known as the “Navidad Current”. Winter warming in the southern Bay of Biscay during Navidad years has been correlated with low values of the NAO index and this current was found to extend from Portugal to Norway in exceptional Navidad years (Garcia-Soto et al., 2002).



141 Modern sea-surface conditions of the SW Iberian margin and Alboran Sea are characterised  
142 respectively by mean annual salinities of 36.5 and 37.1 psu (world dataset atlas compiled by  
143 Schmidt, 1999 and Bigg and Rohling, 2000, <http://data.giss.nasa.gov/o18data>: Craig and Gordon  
144 dataset for the Iberian margin and C. Pierre dataset for the Alboran Sea), February SSTs are  
145 around 15.2 and 14.7°C, respectively, and August SSTs are around 20 and 23.7°C (WOA 2001).

### 3. Methodology

#### 3.1. Chronostratigraphy

Cores MD95-2043 (central Alboran Sea) and MD95-2042 (SW Iberian margin), characterised by high sedimentation rates, are composed mainly of calcareous hemipelagic clays and have yielded high resolution paleoceanographic records (e.g. Cacho et al., 1999 and Shackleton et al., 2000, respectively).

The age model of core MD95-2042 is derived from 16 AMS  $^{14}\text{C}$  dates and, for the period beyond AMS  $^{14}\text{C}$  range, by graphical tuning of the MD95-2042 planktonic  $\delta^{18}\text{O}$  record with Greenland ice core  $\delta^{18}\text{O}$  records. The GISP 2 chronology (Bard et al., 2004) was used between 26 and 47 ka, and the GRIPSS09sea chronology (Shackleton et al., 2004) was applied between 47 and 77 ka. Further details of the age models are given in Daniau et al. (2007) and Sánchez-Goñi et al. (2008).

The age model of core MD95-2043 is based on 21 AMS  $^{14}\text{C}$  dates and graphical tuning of the MD95-2043 alkenone SST record to GISP2  $\delta^{18}\text{O}$  (Cacho et al., 1999). Due to the recent improvement of the chronology of the SW Iberian margin core, some discrepancies in the two age models appear in the dates of the climatic events at around 40 ka BP. In these cases, we have slightly modified the chronology of the Alboran Sea record for the time interval between 40 and 50 ka, according to Sánchez-Goñi et al. (2009), in order to align the latter sedimentary sequence with that of the SW Iberian margin.

#### 3.2. Dinoflagellate analysis

Dinoflagellates are flagellate protists that occur in both marine and freshwater environments, and which thrive in the depth range of 18-100 m in oceanic domains (Dodge and Harland, 1991; Raine et al., 2002) and 0-10 m at the coastline. Water turbulence is greater in the neritic zone and represents a limiting factor for light penetration and thus the maximum depth of dinoflagellate habitats. Dinoflagellates reproduce primarily through fission, but sexual reproduction also occurs resulting in a resting cyst which is preserved in sediments (Dodge et Harland, 1991; Head, 1996). The distribution of dinoflagellate cysts (dinocysts) reflects physico-chemical parameters of the overlying water masses (temperature, salinity, sea-ice cover, seasonality and nutrient availability) (e.g. Turon, 1984; Mudie, 1992; Matthiessen, 1995; Rochon et al., 1999; Devillers and de Vernal, 2000; Zonneveld et al., 2001; Marret and Zonneveld, 2003; de Vernal and Marret, 2007).

Dinocyst analysis is therefore an essential tool for reconstructing Quaternary paleoenvironments (e.g. Turon, 1984; Turon and Londeix, 1988; Eynaud et al., 2000, 2004, 2009; de Vernal et al., 1997, 2001, 2005; Mudie et al., 2002, 2004; Grøsfjeld et al., 2006; Penaud et al., 2008, 2009, 2010).

Dinocyst assemblages were characterised at the species level on the sediment fraction smaller than 150  $\mu\text{m}$  on 61 palynological slides for core MD95-2043 (this study) and on 71 slides for core MD95-2042 (Eynaud, 1999; Sánchez-Goñi et al., 2000). The preparation technique followed the protocol described by de Vernal et al. (1999) and Rochon et al. (1999), slightly modified at the EPOC laboratory (Castera and Turon, [http://www.epoc.u-bordeaux.fr/index.php?lang=fr&page=eq\\_paleo26](http://www.epoc.u-bordeaux.fr/index.php?lang=fr&page=eq_paleo26)). Each subsample of 8  $\text{cm}^3$  was weighed, dried overnight and then weighed again to obtain dry weight. Subsamples were then washed through a 150  $\mu\text{m}$  sieve and the fraction smaller than 150  $\mu\text{m}$  was used for palynological analysis. After chemical and physical treatments (cold HCl, cold HF and sieving through single-use 10  $\mu\text{m}$  nylon

mesh screens), the final residue was mounted between slide and coverslip with glycerine jelly coloured with fuschin. Identifications and counts were performed using a Leica DM 6000 microscope at  $400\times$  magnification, and counts aimed to reach 300 specimens wherever possible for each sample (cf. Appendix A). Taxonomic identifications are consistent with those of Fensome et al. (1998) and Fensome and Williams (2004). *Brigantedinium* cysts are grouped together and include all spherical brown cysts, since it is rarely possible to identify them at the species level due to their crumbled aspect which masks the archeopyle. Dinocyst assemblages were described by the percentages of each species calculated on the basis of the total dinocyst sum including the few unidentified taxa and excluding pre-Quaternary cysts. Palynomorph concentrations were calculated using the marker grain method (de Vernal et al., 1999). Aliquot volumes of *Lycopodium* spores were added to each sample before chemical treatments in order to obtain palynomorph concentrations.

### 3.3. Quantitative reconstructions of sea-surface parameters

#### 3.3.1. Dinocyst SST and SSS reconstructions

We used a transfer function based on the Modern Analogue Technique (MAT) to reconstruct sea-surface hydrological parameters from dinocysts. The MAT principally uses the statistical distance between fossil (paleoceanographic record) and current (modern database) assemblages. The calculation of past hydrological parameters relies on a weighted average of the SST values of the best modern analogues found (minimum and maximum number of analogues imposed in the transfer functions are 5; cf. Appendix B for the list of analogues found for each sample). The

maximum weight is given for the closest analogue in terms of statistical distance. The reader is referred to Guiot and de Vernal (2007) for a review of theory of transfer functions and to de Vernal et al. (2001, 2005) for a step by step description of the application of transfer functions to dinocysts, including discussion about the degree of accuracy of the method.

The dinocyst transfer function used in this work (cf. de Vernal et al., 2005; GEOTOP website: [http://www.unites.uqam.ca/geotop/monographie\\_n940/eng/index.shtml](http://www.unites.uqam.ca/geotop/monographie_n940/eng/index.shtml)) is derived from a modern database comprising 60 dinocyst species and 940 stations from the North Atlantic, Arctic and North Pacific oceans and their adjacent seas, including the Mediterranean Sea (84 stations including station “M1039”, cf. Fig. 1; Mangin, 2002), as well as epicontinental environments such as the Estuary and Gulf of St. Lawrence, the Bering Sea and the Hudson Bay. The transfer function (n=940) is run under the “3Pbase” software (Guiot and Goeury, 1996). This software was originally developed for pollen-based quantitative climate reconstruction (<http://www.imep-cnrs.com/pages/3pbase.htm>) and was subsequently applied to dinocyst assemblages (e.g. de Vernal et al., 2001, 2005). An index “Dmin”, provided by the software “3PBase”, allows testing the reliability of the reconstructions (cf. de Vernal et al., 2005). This index describes, for each sample analyzed, the distance between the closest analogue found by the transfer function and the fossil assemblage. A threshold value is calculated from the calibration of the database for the identification of non-similar or very bad analogues. This threshold value provided by the software “3PBase” is 71.72 and, below this value, the similarity between the modern data and the fossil record is considered significant (cf. Appendix B for the Dmin values calculated for each sample). The authors caution that the full reference set has been used for the calculations of hydrological parameters without any regional selection of samples within the modern database. In this study, we present February and August mean sea-surface temperatures (SST, with prediction

errors of  $\pm 1.2^{\circ}\text{C}$  and  $\pm 1.8^{\circ}\text{C}$  respectively), and February and August mean sea-surface salinities (SSS, with prediction errors of  $\pm 1.7$  for both).

### 3.3.2. Foraminiferal SST and SSS reconstructions

In the same way, we used a transfer function based on the MAT to reconstruct foraminiferal SST from the foraminiferal assemblages of cores MD95-2042 (Cayre et al., 1999) and MD95-2043 (Pérez-Folgado et al., 2003). Calculation of past hydrological parameters relies on a weighted average of the SST values of the best 5 modern analogues found systematically. This transfer function has been developed at EPOC laboratory (“Environnements et Paléoenvironnements OCéaniques”, Bordeaux1 University, France). The MAT (e.g. Kucera, 2007) is run under the “R” software using a script first developed for dinocyst transfer functions ([http://www.cerege.fr/IMG/pdf/ECCOR\\_StatRAvr08.pdf](http://www.cerege.fr/IMG/pdf/ECCOR_StatRAvr08.pdf)). The modern database relies on a modern database of 1007 modern assemblages and is derived from the ones developed separately for the North Atlantic and the Mediterranean seas during the MARGO project (Kucera et al., 2005; Hayes et al., 2005). These databases were merged together to offer a larger set of analogues for subtropical reconstructions over the last glacial period notably (Eynaud et al., 2009; Matsuzaki et al., in press). Modern hydrological parameters were requested from the WOA 2008 database using the tool developed during the MARGO project (<http://www.geo.uni-bremen.de/geomod/staff/csn/woasample.html>). This method allows the reconstruction of annual and seasonal (winter, spring, summer and fall) SST. In this paper, we present winter and summer mean SST with a prediction error of  $\pm 1.2^{\circ}\text{C}$  and  $\pm 1.3^{\circ}\text{C}$  respectively, and annual SST with a prediction error of  $\pm 1.1^{\circ}\text{C}$  (Eynaud et al., 2009; Matsuzaki et al., in press).

SSS estimates have been derived using the approach summarised in Malaizé and Caley (2009) for calibration of the salinity-water isotope relationship. Craig and Gordon (1965) established the first salinity-water isotope relationship as follows:

$$\delta^{18}\text{O}_{\text{sw}} = 0.66 \text{ SSS} - 23.5$$

Since this pioneer work, many measurements have been performed and many different relationships, with different slopes, have been derived for different oceans (Ostlund et al., 1987, Schmidt, 1999; LeGrande and Schmidt, 2006). Discrepancies in slope and in intercept values are due to local characteristics, on spatial and temporal scales. For the Atlantic Ocean, an important dataset, established from several decades of oceanographic measurements, allows revision of the Craig and Gordon (1965) calibration and the determination of a new relationship, with a mean slope component of 0.558.

In order to estimate past changes in oceanic  $\delta^{18}\text{O}_{\text{sw}}$ , Epstein et al. (1953) established a paleotemperature equation which links temperature with the isotopic composition of calcite ( $\delta^{18}\text{O}_{\text{c}}$ ) in calcareous shells (e.g. foraminifera) and the ambient waters ( $\delta^{18}\text{O}_{\text{sw}}$ ). Shackleton and Opdyke (1973) have adapted the equation of Epstein et al. (1953) as follows:

$$T = 16.9 - 4.38 (\delta^{18}\text{O}_{\text{c}} - \delta^{18}\text{O}_{\text{sw}}) + 0.13 (\delta^{18}\text{O}_{\text{c}} - \delta^{18}\text{O}_{\text{sw}})^2$$

Stable isotope  $\delta^{18}\text{O}_{\text{c}}$  measurements in cores MD95-2042 (Cayre et al., 1999; Shackleton et al., 2000) and MD95-2043 (Cacho et al., 1999) were carried out on *G. bulloides* monospecific samples. Following the pioneer study of Duplessy et al. (1991), we corrected the summer temperature by 1°C for *G. bulloides* species. By solving the Shackleton and Opdyke (1973) equation, we obtain  $\delta^{18}\text{O}_{\text{sw}}$  variations, which integrate the signal of both local and global variations. To remove the global influence of continental ice volume, we used estimations of past global  $\delta^{18}\text{O}_{\text{sw}}$  changes based on benthic isotopic records and coral terrace growth (Waelbroeck et

288 al., 2002), and used the modern  $\delta^{18}\text{O}_{\text{sw}}$  values (1.2 ‰ for the Alboran Sea and 0.97 ‰ for the  
289 Iberian margin) extracted from the world dataset atlas compiled by Schmidt (1999) and Bigg and  
290 Rohling (2000) (C. Pierre dataset for the Alboran Sea, and Craig and Gordon dataset for the  
291 Iberian margin, from <http://data.giss.nasa.gov/o18data>). The residual  $\delta^{18}\text{O}_{\text{sw}}$  “ice-corrected”  
292 signal is then converted into quantitative SSS values for both cores, using a mean slope of 0.558.  
293 SSS uncertainties of around 1 psu derive from the prediction error of the foraminiferal SST  
294 reconstructions (1.8°C uncertainty linked with August SST reconstructions corresponds to a 0.45  
295 ‰ uncertainty on a  $\delta$  scale), as well as on uncertainties in the global  $\delta^{18}\text{O}_{\text{sw}}$  changes linked to  
296 sea level changes (0.15 ‰).



#### 4. Dinocyst assemblages through time

Concerning the species of the genus *Brigantedinium* spp., round brown cysts formed by heterotrophic dinoflagellates, it is important to take into account the fact that high occurrences of *Brigantedinium* spp. can be linked to better preservation under hypoxic or anoxic bottom conditions (Combourieu-Nebout et al., 1998; Zonneveld et al., 2001; Kodrans-Nsiah et al., 2008). We can not exclude that *Brigantedinium* spp. may have been subjected to dissolution since deep ventilation in the western Mediterranean Sea (and thus oxidation processes) during GS was stronger than during GI of the last glacial (cf. benthic  $\delta^{13}\text{C}$  in Fig. 4; Cacho et al., 2006). However, *Brigantedinium* spp. are present throughout the Alboran core without any clear trend between few percentages during GS and high percentages during GI. We can thus expect to reconstruct dinocyst assemblages without significant preservational problems. When comparing both cores (Fig. 2), we note extremely high relative abundances of *Brigantedinium* spp. (30-89%) on the SW Iberian margin (Fig. 2b). This may reflect the high productivity induced by permanent or intensified upwelling cells along the Portuguese margin during the last glacial (e.g. Abrantes, 2000; Lebreiro et al., 1997); this zone today is characterised by a seasonal upwelling system (Peliz et al., 2005) and *Brigantedinium* spp. percentages only reach a maximum of 2-5% in the modern database. Percentages of these cysts fluctuate more in the Alboran Sea, with pronounced oscillations (average of 19% and peaks reaching 30 to 45%) (Fig. 2a).

##### 4.1. Dinocysts occurring during Greenland Stadials

Dinocysts which feature prominently during GS include *Bitectatodinium tepikiense*, *Spiniferites lazus*, *Spiniferites elongatus*, *Impagidinium aculeatum*, and *Operculodinium centrocarpum* in the Alboran Sea (Fig. 2a), and *B. tepikiense*, *S. elongatus*, cysts of *Pentapharsodinium dalei*, *Lingulodinium machaerophorum* and *Nematosphaeropsis labyrinthus* on the SW Iberian margin (Fig. 2b). It is also interesting to note that maximal dinocyst concentrations occur during GS off Portugal (most notably during HS 4; Fig. 2b) contrarily to what we observe in the Alboran record (Fig. 2a).

In the Alboran Sea, *B. tepikiense* increases during HS events, especially HS 3 and HS 4 (Fig. 2a), whereas it occurs during each GS on the SW Iberian margin, where it consistently makes up almost 10% of the total dinocyst assemblage (Fig. 2b). Today, *B. tepikiense* is mainly distributed between 40°N and 60°N in temperate to sub-arctic environments of the North Atlantic, with the highest abundances found south of the Gulf of St. Lawrence in coastal environments of Nova Scotia and the Gulf of Maine (Wall et al., 1977; Mudie, 1992). This species is characteristic of areas marked by strong seasonal contrasts, with freezing winter SSTs and up to 16°C summer SST (Rochon et al., 1999; de Vernal et al., 2005), and enhanced surface water stratification (Rochon et al., 1999; Marret and Zonneveld, 2003). Previous results from the North Atlantic (Zaragosi et al., 2001; Penaud et al., 2009), the SW Iberian margin (Sánchez-Gómez et al., 2000; Turon et al., 2003), and the western Mediterranean Sea (Turon and Londeix, 1988; Combourieu-Nebout et al., 2002) have shown increased abundances of *B. tepikiense* during HS.

*S. elongatus* develops during each GS with low percentages reaching 2-5% in the Alboran Sea (Fig. 2a) and 1-2% on the western Iberian margin (Fig. 2b). Maximum present-day occurrences of this species are observed in the Baffin Bay and Barents Sea, and this taxon is generally related

to cool to temperate conditions (Rochon et al., 1999). The significant occurrence of *B. tepikiense* and *S. elongatus* is attributed to strong seasonality characterised by winter sea-surface temperatures probably less than 5°C (Marret et al., 2004).

Cysts of *P. dalei* occur sporadically in the Alboran Sea core (Fig. 2a) but mark clearly the cold events in core MD95-2042, most notably HS 2 and HS 4 (Fig. 2b). Cysts of *P. dalei* are well represented in modern sediments from polar to subpolar environments that experience summer sea-surface temperatures higher than 4°C (Rochon et al., 1999; Matthiessen, 1995; Marret et al., 2004; de Vernal et al., 2005). They are particularly prevalent as part of the spring bloom within North Atlantic fjord systems (Dale, 1977; Harland et al., 2004a,b).

In the Alboran Sea, we show that *S. lazus* is associated with cold HS and especially HS 5 (Fig. 2a). Today, the distribution of *S. lazus* is restricted to coastal regions of western Europe, always with low abundances (less than 2% of the dinocyst assemblages) (Reid, 1974). This species can be regarded as a neritic temperate species of regions characterised by oligotrophic to eutrophic surface water conditions (Reid, 1974; Harland, 1983).

Finally, the most striking feature visible in the dinocyst distribution during the D-O cycles is the systematic occurrence of *Impagidinium aculeatum* during GS in the Alboran Sea, with low percentages reaching a maximum of 5% (Fig. 2a). On the western Iberian margin, this species peaks during GI, although a local maximum is also observed during HS 5 (Fig. 2b). At present, this taxon is associated with warm water dinocyst assemblages; high relative abundances are found in tropical/subtropical oligotrophic open oceanic sites (Turon, 1984). In SW Iberian and western Mediterranean paleoclimate records, this species is characteristic of the Holocene with

percentages close to 20% (Combourieu-Nebout et al., 1998; Turon et al., 2003; Rouis-Zargouni et al., 2010). However, percentages close to 5% were also previously observed during cold stadials (HS 1 and HS 2) in a core from the Sicilian-Tunisian Strait (Rouis-Zargouni et al., 2010).

#### 4.2. Dinocysts occurring during Greenland Interstadials

Dinocysts which feature prominently during GI in the Alboran Sea include *Spiniferites mirabilis*, *Impagidinium patulum*, *L. machaerophorum*, *N. labyrinthus* as well as some heterotrophic species (Protoperidinioids, *Selenopemphix nephroides* and *Selenopemphix quanta*, but excluding *Brigantedinium* spp. whose ecology is rather complex) (Fig. 2a). On the SW Iberian margin they include *Impagidinium* species (*I. aculeatum* and *I. patulum*), *S. mirabilis*, *O. centrocarpum* and *S. nephroides* (Fig. 2b). Unlike the SW Iberian margin (Fig. 2b), maximal dinocyst concentrations occur during GI in the Alboran Sea (especially during GI 8 and GI 12; Fig. 2a).

In the Alboran Sea, GI are characterised by the species *S. mirabilis* (Fig. 2a) with percentages on average four times higher than on the SW Iberian margin (Fig. 2b). The highest relative abundances of *S. mirabilis* are recorded during GI 7 and GI 8. Today, *S. mirabilis* is mainly distributed between 35°N and 50°N in warm temperate to temperate environments of the North Atlantic with highest occurrences found off the coast of Portugal and in the Bay of Biscay (Rochon et al., 1999). This species extends as far south as 10°N and is generally absent from areas with summer SST below 12°C and salinity below 28.5, and thrives optimally when winter SSTs are between 10°C and 15°C and summer SSTs are above 15°C.

On the SW Iberian margin, GI are characterised by *I. patulum* (Fig. 2b) with abundances four

times higher than in the Alboran Sea (Fig. 2a). Most *Impagidinium* species occur today with maximum frequencies in tropical to warm temperate waters between 20°N and 35°N and are representative of full-oceanic conditions (Harland, 1983; Turon, 1984; Bouimetarhan et al., 2009).

*Spiniferites delicatus* is common on the SW Iberian margin and is mainly linked with interstadial conditions (Fig. 2b), while it is rare in the Alboran Sea (Fig. 2a). *S. delicatus* is a temperate species adapted to warm and neritic conditions (Wall et al., 1977; Harland, 1983; Marret, 1994).

*S. quanta*, *S. nephroides* and some Protoperidinioids show a distribution pattern closely linked to GI in the Alboran Sea (Fig. 2a). This association also holds for *S. nephroides* on the SW Iberian margin, but is less obvious for *S. quanta* and Protoperidinioids as they also increase during GS (Fig. 2b). These latter taxa, represented by low relative abundances in the modern database and a scattered distribution in the North Atlantic (Rochon et al., 1999), are derived from heterotrophic dinoflagellates and are mainly related to high food resources. Their heterotrophic strategy of nutrition probably links them to the presence of higher concentrations of nutrients in surface waters. *S. quanta* has previously been linked to the dynamics of upwelling cells off NW Africa (Dodge and Harland, 1991; Penaud et al., 2010).

#### **4.3. Opposite dinocyst patterns between Iberian and Alboran environments over D-O cycles**

Other dinocyst species not described above, *L. machaerophorum*, *N. labyrinthus*, and *O. centrocarpum*, are an important component of the dinocyst assemblages and show opposite patterns in both cores

*N. labyrinthus* shows very high percentages in the Alboran Sea (average 24%), where it occurs generally within GI (Fig. 2a). Peaks of this species systematically exceed 40% and can reach 60 to 70% of the total dinocyst assemblage. On the SW Iberian margin, this taxon is less prevalent (average of 4.5%) with peaks generally reaching 10% during GS (except during HS) (Fig. 2b). At present, *N. labyrinthus* is a typical open-ocean species found predominantly between 45°N and 65°N in the North Atlantic Ocean (Rochon et al., 1999; Matthiessen, 1995; Marret et al., 2004; de Vernal et al., 2005). Maximum abundances of this species are recorded off southern Greenland where cold waters from the East Greenland and Labrador currents mix with warm North Atlantic waters of the Irminger Current (Rochon et al., 1999; Marret et al., 2004). This species, in association with *B. tepikiense*, was previously related to polar water incursions during MIS 5 cold substages off Portugal (Sánchez-Goñi et al., 1999; Eynaud et al., 2000), and during the Younger Dryas off Portugal (Turon et al., 2003), in the Mediterranean (Turon and Londeix, 1988; Rouis-Zargouni et al., 2010) and off NW Morocco (Marret and Turon, 1994; Penaud et al., 2010). *N. labyrinthus* has also been positively correlated with nutrient-rich and cool waters (Turon and Londeix, 1988; Devillers and de Vernal, 2000).

*L. machaerophorum* occurs during GI in the Alboran Sea, particularly GI 8, 9 and 12 (Fig. 2a), while it occurs during GS on the SW Iberian margin (Fig. 2b). *L. machaerophorum* is today considered to be a temperate to tropical coastal euryhaline species (Mertens et al., 2009). It dominates associations from the northern African and southern European Atlantic shelves, and it is also found in abundance in North African coastal upwelling regions (Targarona et al., 1999; Sprangers et al., 2004) and near the Congo outlet (Marret, 1994). Extremely high concentrations of these cysts have been found in areas with typical seasonally stratified water columns such as

fjords, bays, and estuaries (e.g. Reid, 1972; Bradford and Wall, 1984; Dale, 1985; Lewis, 1988; Morzadec-Kerfourn, 1988; Dale et al., 1999). This taxon has often been related to warm and stratified surface waters (Marret and Zonneveld, 2003), and has also been used as a proxy for fluvial inputs towards the ocean (Zaragosi et al., 2001; Holzwarth et al., 2010).

*O. centrocarpum* occurs frequently in the Alboran Sea record with percentages reaching 20 to 40% during almost every GS (Fig. 2a). On the SW Iberian margin, this species shows relatively low percentages, with peaks generally less than 10% during GI and reaching a maximum of 20% during GI 3 (Fig. 2b). This species is considered to be a cosmopolitan, cool to temperate taxon (Turon, 1984; Rochon et al., 1999; Marret and Zonneveld, 2003), and an abundance pattern following the route of the North Atlantic Drift (NAD) has been identified from its present geographical distribution in North Atlantic surface sediments (Turon, 1984; Rochon et al., 1999). This observation was previously used to interpret the presence of an active NAD at times when this species was abundant in the Quaternary North Atlantic sediments (Zaragosi et al., 2001; Eynaud et al., 2004; Penaud et al., 2008, 2009).

## **5. Temperature and salinity records: convergences and discrepancies**

### **5.1. SST: dinocysts *versus* planktonic foraminifera**

Quantitative reconstructions derived from the two transfer functions (dinocyst and foraminifera) are not directly comparable since the reconstructed parameters are not exactly the same. The dinocyst transfer function 3PBase-940 only provides February and August SST reconstructions while the foraminiferal transfer function R-1007 only provides annual and seasonal-mean (i.e.

winter, spring, summer and fall) SST reconstructions. However, February and August foraminiferal SST can be estimated using the MAT transfer function derived from Pflaumann et al. (1996) which relies on a modern database of 692 modern assemblages (only Atlantic stations), improved during the MARGO project (Kucera et al., 2005). It is, however, more appropriate for us to discuss the foraminiferal data from the R-1007 transfer function (Atlantic and Mediterranean modern databases) for the Alboran Sea core which is located at the boundary of the two basins. The comparison of winter *versus* February SST values on the 664 common stations from the foraminiferal north Atlantic databases (n=1007 *versus* n=692) generates a mean difference of 0.26°C (with a maximum difference of 1.95°C). For the summer *versus* August SST values, the mean difference is 0.37°C (with a maximum difference of 1.1°C). These values are within the range of the error bars of the foraminiferal reconstructions and therefore encourage us to consider that monthly and seasonal foraminiferal SST values can be discussed interchangeably. Concerning dinocysts, the n=940 database also includes Mediterranean stations. It is worth noting that, among the 84 Mediterranean analogues (including 17 stations in the Alboran Sea), the only Mediterranean analogue found by the transfer function is located in the Alboran Sea and named “M1039” (Fig. 1; Appendix B). This is mainly the case during GI conditions (GIs 3, 5, 7, 8, 9, 11, 12 and 13; cf. Appendix B), suggesting that GI conditions in the Alboran Sea between 25 and 50 ka were roughly equivalent to conditions prevailing at the “M1039” site today (Fig. 1).

When comparing SST reconstructions from both micropaleontological proxies on the two cores, one can note that February *versus* winter SST values obtained with dinocysts (3PBase-940) and foraminifera (R-1007), respectively, are closer than August *versus* summer ones (Fig. 3). However, the general good consistency of February *versus* winter SST is not valid for the SW Iberian margin during HS 5 with about 8°C difference between both micropaleontological



reconstructions (dinocyst SST estimates around 13°C and foraminiferal ones close to 5°C; Fig. 3). This offset is unrealistically large given the prediction error for each method (around 1.2°C). This minor SST drop expressed in dinocyst populations may be underestimated, as also revealed by the annual alkenone-derived SST values warmer than the February dinocyst-based SST ones (Fig. 3). One reason may come from the occurrence of the dinocyst species *Impagidinium aculeatum* during HS 5 (Fig. 2). Indeed, on the western Iberian margin, this species peaks during GI, although a local maximum is observed during HS 5 (percentages slightly higher than 5%). However, this species is associated with warm water dinocyst assemblages and is found today in tropical/subtropical oligotrophic open oceanic sites (Turon, 1984). Although the occurrence of this taxon during a cold HS is not understood, it may switch the transfer function towards warmer SST values.

August *versus* summer SST reconstructions for both cores show similar overall trends but differ more in terms of amplitudes, with dinocyst SSTs being 5 to 10°C higher than foraminiferal SST estimates (Fig. 3). Two hypotheses can be put forward with respect to this observation. Either the August/summer (dinocyst or/and foraminiferal) quantifications are less reliable or the discrepancy reflects an ecological bias. Dinocysts are indeed produced by dinoflagellates that thrive in the photic zone while foraminifera can migrate deeply in the water column with living depths ranging from 0 to 1000 m. Dinoflagellates, being found in shallower water, would thus record warmer SST consistently with a higher stratification during the warmest month, i.e. August. Various biases between different micropaleontological reconstructions can thus occur in relation to the ecological strategy (depth of habitat and growth seasons) of the different planktonic populations (de Vernal et al., 2005). The following comparison with alkenones will help us to decipher whether the foraminiferal or dinocyst signal is too cold or warm, respectively.

Finally, concerning the Alboran Sea core, one can note that dinocysts and foraminiferal show closer August *versus* summer SST values between 31 and 38 ka and larger offsets between 38 and 50 ka. This point will be further discussed in section 6.2.3. of this manuscript.

## **5.2. SST: transfer functions *versus* alkenones**

Alkenone-derived SST from cores MD95-2043 (Cacho et al., 1999) and MD95-2042 (Pailler and Bard, 2002) has previously been compared with ice-core records, demonstrating a close linking between SSTs in the western Mediterranean and temperature developments over the wider North Atlantic region, including Greenland. Here, it appears that our dinocyst-based SST reconstructions for both cores match peak to peak with the SSTs derived from alkenones, showing minimum values during GS (Fig. 3). Furthermore, the alkenone-based SST, which records an annual signal of temperature, fluctuates systematically in between the temperature range given by seasonal dinocyst SST reconstructions and is closer to February than August SST (Fig. 3). A co-variation between February dinocyst SST and alkenone-derived SST reconstructions was previously observed off NW Morocco during the last glacial over the last 30 ka (Penaud et al., 2010). This would confirm the hypothesis that switches in mean annual temperatures were dominated by, and thus weighted towards, the winter season during the last glacial cycle as suggested by Denton et al. (2005).

The foraminiferal transfer function  $n=1007$  also provides annual SST reconstructions that can directly be compared with the alkenone signal. One can note that annual SST values reconstructed with both proxies are closer during GI than during GS (Fig. 3). Foraminifera routinely provide much colder temperatures during GS, and especially during HS that are

characterised by significant SST anomalies between 4 and 7°C (Fig. 3). This shift of annual SST values towards cold SSTs is mainly due to extremely cold summer SSTs reconstructed with foraminifera during GS (Fig. 3). This contrast has parallels to the previous observation on the considerable offsets between dinocyst and foraminiferal August *versus* summer SST. Since alkenones are synthesised by coccolithophorids which are single-celled algae, protists and phytoplankton such as dinoflagellates, we can assume that they both give a signature of sea-surface hydrological changes occurring in the photic zone, while foraminifera may yield a bias towards colder SSTs, especially during GS. However, it will be crucial to understand if this finding reflects a real ecological strategy of foraminifera (different depths of habitat following different seasons) or a problem associated with the transfer function.

### 5.3. SSS: dinocysts *versus* planktonic foraminifera

Quantifications of salinity are of critical interest as they are fairly rare in paleoclimate studies. A major challenge in paleoceanography is to increase the availability of SSS reconstructions for comparison with climate models (e.g. MARGO project members, 2009). In our records, similar changes, both in amplitude and timing, are revealed through the comparison of February dinocyst-based SSS *versus* winter foraminiferal derived ones (Fig. 3). Numerical results are always very close or at least within the prediction error of 1-1.8 psu, except during HS 5 and GI 12 at the SW Iberian margin which are marked by differences of 2 to 3 psu between both micropaleontological proxies (Fig. 3). Comparison of the February/winter SSS data is particularly striking because the methods of quantification are different. One method requires MAT calculation of SST based on planktonic foraminifera and  $\delta^{18}\text{O}$  analysis (e.g. Malaizé and

Caley, 2009), while the other one is obtained on the basis of MAT transfer function applied to dinocyst assemblages (e.g. de Vernal et al., 2005). However, correlations between fluctuations in August dinocyst-based SSS and summer foraminiferal derived ones are less evident with fluctuations similar in timing but divergent in terms of amplitudes, especially for the Alboran Sea (Fig. 3).

For the SW Iberian margin, our study shows that major low salinity events are recorded during HS (Fig. 3b). HS 4 displays the maximum drop in February/winter SSS with values reaching 31 psu, corresponding to the largest fluxes of freshwater to the ocean over our study period. Our data for HS 3 (around 31.5-32.5 psu, 4 psu lower than the modern value) also show a major low salinity event and are consistent with previous results acquired further north along the Celtic margin over the last 35 ka BP where this interval was also characterised by a 4 psu depletion in SSS (Eynaud et al., submitted).

For the Alboran Sea, the difference in the resolution of analysis between dinocyst and foraminiferal/isotope reconstructions makes it difficult to compare some sections (Fig. 3a). This is mainly due to the fact that foraminiferal SSS is calculated from both foraminiferal SST and planktonic  $\delta^{18}\text{O}$  data and the resolution of the  $\delta^{18}\text{O}$  record is lower than the foraminiferal SST record. For the whole Alboran Sea record, February/winter SSS shows changes of similar order of magnitude between each GS, with the strongest signal of freshening recorded during HS 4 reaching 33 psu (4 psu lower than the modern value).

## **6. Paleohydrological changes affecting subtropical Atlantic latitudes through D-O cycles**

## **6.1. The new contribution of dinocyst assemblages in the Alboran Sea**

### **6.1.1. Warm intervals (GI) in the Alboran Sea**

During GI, we observe an expansion of warm temperate to tropical species with a trend of decreasing abundance, and decreasing February and alkenone SST, from immediately prior to a Heinrich Stadial to the next HS (Fig. 4). This pattern is similar to that seen in the Greenland ice core isotope records showing progressively shorter GI and smaller increases in Greenland air temperatures between HS 5 and HS 4 and between HS 4 and HS 3 (Fig. 4, NGRIP GICC05). This demonstrates a similar trend between Alboran SST and atmospheric temperatures over Greenland, involving a rapid transmission of Northern Atlantic climate changes into the western Mediterranean region.

When comparing the amplitude of warm taxa development during individual D-O warming (Fig. 4), we note less frequent occurrences of thermophilous taxa during the earlier interstadials (GI 12-9) than during the subsequent interstadials (GI 8-5). This is consistent with pollen analysis conducted on the same core (Fletcher and Sánchez-Goñi, 2008) demonstrating high values for Mediterranean forest during GI 8, 7, 6 and 5 reflecting the maximum in subtropical summer insolation associated with the precession minimum centred around 30-35 ka (Fig. 4). Such a development is also seen in paleo-vegetation records at nearby Alboran site ODP 976 (Combourieu-Nebout et al., 2002) and on the SW Iberian margin (MD95-2042: Sánchez-Goñi et al., 2000).

The interstadials GI 8 and GI 12, immediately succeeding HS 4 and HS 5, respectively, exhibit particularly long and warm periods. They are both marked by high relative abundances of warm water dinocysts, high SST estimates (especially clear with alkenones; Fig. 4), and by the highest

paleoproductivity conditions indicated by heterotrophic taxa in the early interstadials and high dinocyst concentrations in the second half of GI 8 and GI 12 (Fig. 4). In terms of sea-surface paleohydrology, GI 8 and GI 12 are thus very similar with a comparable bipartite structure (Fig. 4). Palynological investigations of GI 8 and GI 12 in the same Alboran Sea core showed that these periods were characterised by the strongest expansions of mixed oak forest between 48 and 15 ka (Fletcher and Sánchez-Goñi, 2008). Furthermore, Fletcher and Sánchez-Goñi (2008) identified an Atlantic oceanic character during GI 12, in contrast to a markedly Mediterranean character during GI 8, linked to the precession minimum that likely enhanced the Mediterranean climate and caused an enhanced seasonal contrast between dry summers and wet winters (Sánchez-Goñi et al., 2008, 2009; Fletcher and Sánchez-Goñi, 2008). Our dinocyst data also reveal a strong expansion of the species *L. machaerophorum* in the second half of GI 8, representing between 20 and 40% of the total dinocyst assemblage (Fig. 4). This species has sometimes been used to trace fluvial inputs (Zaragosi et al., 2001; Holzwarth et al., 2010) and could reflect higher river run-off to the Alboran Sea, providing further evidence for increased winter precipitations during this interval.

Throughout our record, heterotrophic dinocyst species (*S. nephroides*, *S. quanta*, and Protoperidinioids cysts) occur during each GI in the Alboran Sea (Fig. 4). Their occurrences suggest sea-surface conditions characterised by increased productivity (Rochon et al., 1999), as also indicated by increased total dinocyst concentrations (Fig. 4). This general pattern of higher productivity during GI relative to GS has previously been discussed based on geochemical evidence (calcium carbonate, barium excess, and total organic carbon) from the same core (Moreno et al., 2004). Today, the two semi-permanent anticyclonic gyres found in the Alboran Sea represent energetic mesoscale features and the main forcing maintaining these gyres is the Atlantic jet which enters through the Strait of Gibraltar (Bormans and Garret, 1989; Benzohra

and Millot, 1995; Garcia-Lafuente et al., 1998; Macias et al., 2008). The intensity of the jet is typically modulated by atmospheric pressure variations over the western Mediterranean. Indeed, when atmospheric pressures are lower than average, configuration close to a NAO negative mode, westerlies prevail above the Mediterranean, the Atlantic jet flows northward near the Spanish coast and the western Alboran gyre is well developed in the entire western Alboran Sea. The opposite (NAO positive mode) occurs when easterly winds prevail, the inflow of Atlantic waters is lower and the Atlantic jet is directed southward, reducing the western Alboran gyre extent (Candela et al., 1989; Garcia-Lafuente et al., 2002; Macias et al., 2008). At an annual scale, on the basis of satellite imagery analysis (e.g. Garcia-Gorriz and Carr, 1999; Baldacci et al., 2001; Macias et al., 2007, 2008) maximum surface chlorophyll concentrations were usually found in winter and minimum values were observed in summer (July and August). Biological patterns are thus also tightly coupled to atmospheric pressure above the Mediterranean Basin with westerlies being shifted southward during winter. At the millennial-scale resolution of our study and in agreement with Moreno et al. (2004), our data suggest that GI conditions would exhibit a prolonged southward shift of the westerly wind belt, inducing a more intense Atlantic surface jet that favoured gyre-induced upwelling in the Alboran Sea.

#### **6.1.2. Cold intervals (GS) recorded in the Alboran Sea**

The association *B. tepikiense* - *S. elongatus* represents an indicator for the incursion of subpolar water masses at the Alboran site that is highly evident during HS (Fig. 4). This latter pattern is similar to that of the subpolar foraminifera *Neogloboquadrina pachyderma* s. recorded in the same core (Cacho et al., 1999) that shows higher percentages during HS (Fig. 4). This foraminifer displays the highest percentages during HS 4, then HS 3 and finally HS 5, while *B.*

654 *tepikiense* shows higher percentages during HS 3 compared to HS 4 (cf. Figs. 2 and 4). *B.*  
 655 *tepikiense* is absent from the Mediterranean Sea today, and highest abundances of this species  
 656 occur in areas characterised by high-amplitude (10°C) seasonal temperature shifts (Rochon et al.,  
 657 1999). Therefore, its occurrence during HS in Alboran Sea surface waters implies enhanced  
 658 seasonal temperature contrast (15°C; cf. Fig. 5) compared to the present-day one (*i.e.* 10°C;  
 659 23.5°C in summer and 14.5°C in winter; cf. Fig. 5), caused by a strong decrease of winter SST  
 660 (Fig. 4). Our February dinocyst SST reconstructions reinforce this hypothesis by showing low  
 661 SST with values around 5.5°C and 6.5°C during HS 4 and HS 3, respectively, *i.e.* 9°C less than at  
 662 present (Fig. 4). It is thus important to note that, in contrast to *N. pachyderma* s., *B. tepikiense*  
 663 does not mark systematically colder intervals but intervals with larger seasonal contrasts. Our  
 664 results are also in agreement with other observations made at ODP Site 976 (Alboran Sea) that  
 665 reflect coeval increases of *B. tepikiense* with *N. pachyderma* s. percentages during HS, over the  
 666 last 50 ka BP (Turon and Londeix, 1988; Combourieu-Nebout et al., 2002). Our data thus  
 667 confirm that sea-surface cooling in the Alboran Sea was mainly linked to the advection of cold  
 668 Atlantic water to the western Mediterranean (Cacho et al., 1999). Such cold-water advection  
 669 occurred synchronously with regional cooling related to atmospheric conditions over the western  
 670 Mediterranean (Combourieu-Nebout et al., 2002; Sánchez-Goñi et al., 2002). Indeed, on the  
 671 adjacent continent, the Mediterranean forest (*i.e.* temperate taxa) collapsed (Fig. 4) and estimated  
 672 winter atmospheric conditions indicate a 10°C lowering and a decrease of 400 mm in  
 673 precipitation (Sánchez-Goñi et al., 2002).  
 674 The HS configuration contrasts with the other GS. In the Alboran Sea, before or during each GS  
 675 (especially those not associated with HS conditions) we note pronounced peaks of *O.*  
 676 *centrocarpum* (Fig. 4). The occurrence of *O. centrocarpum* in the Alboran Sea, whose present-  
 677 day distribution directly mirrors the flow path of the NAD, may result from the influx of cool



North Atlantic waters entering into the Mediterranean; temperatures of these waters, while presumably low, remained above those of the subpolar waters that entered the Mediterranean during HS. GS events of the last glacial have been demonstrated to coincide with intensification of the deep circulation in the Mediterranean (Cacho et al., 2000, 2006; Sierro et al., 2005; Frigola et al., 2008). Our data suggest that the intensification of deep ventilation in the Alboran Sea, reflected in benthic  $\delta^{13}\text{C}$  data (Fig. 4; Cacho et al., 2006), was synchronous with the advection of North Atlantic waters to the Mediterranean, as reflected by highest relative abundances of cool-water dinocyst taxa (Fig. 4).

We demonstrate two different patterns during GS: those associated with HS are marked by increased abundances of cold water species associated with subpolar waters, and those not associated with HS are marked by an expansion of cool North Atlantic species. Interestingly, it has been demonstrated that the densest Western Mediterranean Deep Water was formed during GS not associated with HS (Cacho et al., 2006; Frigola et al., 2008). More precisely, it has been suggested that a strong mode of overturning prevailed during GS not associated with HS, an intermediate mode of overturning during HS and a weak mode of overturning during GI (Sierro et al., 2005; Frigola et al., 2008). Strong overturning was expected during HS since strong and cold northern continental winds prevailed over the Mediterranean resulting in dry-cold conditions on land (Fig. 4; Combourieu-Nebout et al., 2002; Sánchez-Goñi et al., 2002). However, the HS intermediate mode has been linked with a strong influence of subpolar waters that lowered sea-surface salinity thus reducing deep water formation and favouring water column stratification (Sierro et al., 2005). The observation of subpolar species (*N. pachyderma* s. and *B. tepikiense*) during HS (especially HS 3 and HS 4), as well as the low winter and summer salinities reconstructed from dinocysts, lowered by around 0.5 to 1.5 psu compared to the other GS in both

seasonal configurations (Fig. 3), within low precipitation phases, reinforce the idea of sustained cold conditions with subpolar water masses advection towards the Mediterranean Sea and decreased deep water formation.

## **6.2. Alboran Sea *versus* SW Iberian margin between 50 and 25 ka**

### **6.2.1. SST reconstructions and paleoenvironmental signatures**

In both cores, lowest SST estimates are observed during HS 4 which represents the most pronounced cold event between 25 and 50 ka, with February/winter SST of about 5.5°C and 4°C recorded in the Alboran Sea and the SW Iberian margin, respectively (Fig. 3). Previously, the coldest deep water temperatures in the Alboran Sea (Cacho et al., 2006), maximum concentrations of IRD off the Portuguese margin (Thouveny et al., 2000), and a significant increase in the transport of Saharan dust (Moreno et al., 2002) were observed to occur during HS 4. This confirms the magnitude of HS 4 (cf. Eynaud et al., 2009) in terms of expansion of polar waters towards the Iberian margin (i.e. February SST 11°C lower than modern ones) and even towards the western Mediterranean (i.e. February SST 9°C lower than modern ones), in phase with a nearly complete shutdown of the thermohaline circulation (Maslin et al., 1995; Elliot et al., 2002; Roche et al., 2004).

HS 3 is marked by a change in surface hydrological conditions with February/winter SST of about 6.5°C in the Alboran Sea and 5.5°C off Portugal (Fig. 3). Winter conditions seem thus to have been less severe during HS 3 than HS 4, although they are nevertheless characterised in both paleo-records by significant cooling.

Finally, HS 5 is the event which displays the weakest changes both in the Alboran Sea and off Portugal, where dinocyst February SST are about 9°C and 13°C, respectively (Fig. 4). However, foraminiferal winter SST estimates are close to 6°C and 5°C in the Alboran Sea and off Portugal, respectively. Quantifications derived from transfer functions appear less reliable during this interval. The alkenone annual signal (around 10.5-11°C in the Alboran Sea and 12-12.5°C off Portugal) probably provide an intermediate signature between dinocyst-based (too warm) and foraminiferal-based (too cold) February/winter SST estimates.

Micropaleontological evidence in the subpolar North Atlantic has shown that abrupt SST changes associated with the D-O events in Greenland were matched by SST variations of at least 3-5°C (Bond et al., 1992, 1993; Elliot et al., 2002). In the subtropical North Atlantic, SST excursions of 4-5°C across stadial-interstadial transitions of the last glacial were recorded from the Bermuda Rise (alkenones: Sachs and Lehman, 1999; isotopes: Keigwin and Boyle, 1999) and off Portugal (alkenones: Bard et al., 2000; Martrat et al., 2007). SST changes of up to 6°C are also documented in the western Mediterranean (alkenones: Martrat et al., 2004), due to southward shifts in the position of the Polar Front. Consistently with these previous results, we show here that the Alboran Sea and the SW Iberian margin experienced fluctuations of dinocyst SST of around 5-6°C between GI and GS, except for HS events and more specifically HS 4 with a SST drop of around 11°C off Portugal and of 8°C in the Alboran Sea. This demonstrates the extreme sensitivity of dinocysts to climate fluctuations in subtropical latitudes.

#### **6.2.2. Multiproxy evidence for paleohydrological changes through time**

During GI, the expansion of the Mediterranean forest (Fig. 4) was attributed to atmospheric

conditions close to present-day ones with warm summer and wet winter conditions over southwestern Europe (e.g. Sánchez-Goñi et al., 2002; Combourieu-Nebout et al., 2002; Bout-Roumazelles et al., 2007; Daniau et al., 2007). During those times, we show that warm temperate species *S. mirabilis* and *I. patulum* expanded in the Alboran Sea and on the SW Iberian margin, respectively (Fig. 4), and high SST is recorded at both sites during GI revealing sea-surface conditions closer to present-day ones (Figs. 3 and 4).

During GS, the decline of the Mediterranean forest (Fig. 4) and the development of steppe and semi-desert vegetation over the south-western European borderlands were attributed to intensified winter dryness with cold continental conditions affecting the western Mediterranean area (e.g. Sánchez-Goñi et al., 2002; Combourieu-Nebout et al., 2002; Moreno et al., 2002, 2005; Roucoux et al., 2005; Bout-Roumazelles et al., 2007; Daniau et al., 2007). At that time, assemblages of cold-water dinocyst species, including *B. tepikiense* and *S. elongatus* developed, reflecting cold-water advection along the SW Iberian margin and towards the Alboran Sea (Fig. 4). However, unlike the western Iberian margin where *B. tepikiense* occurs during each GS, *B. tepikiense* expands principally in the Alboran Sea during HS, and especially during HS 3 and HS 4. In the western Mediterranean Sea, HS impacts were therefore greater than those associated with the other GS. Broecker (2006) has compiled data from several areas and has identified sites where the impact associated with North Atlantic Heinrich events is larger (eastern Brazil, central Florida, Arabian Sea, Chinese stalagmites, and western Mediterranean area), in contrast to sites where impacts are similar to those observed during the other stadials (Greenland ice and Cariaco Basin). To explain this discrepancy, Broecker (2006) involves the greater magnitude of north-hemispheric sea ice expansion associated with North Atlantic Heinrich events which exceeded that associated with the other stadials.

772 *B. tepikiense* was previously used to trace subpolar water masses on the western Iberian margin  
773 (Eynaud et al., 2000; Turon et al., 2003) and in the Alboran Sea (Turon and Londeix, 1988;  
774 Combourieu-Nebout et al., 2002) during HS. In our data, the observation of subpolar dinocysts in  
775 both cores, in phase and synchronous with peaks of *N. pachyderma* s. (Fig. 4), confirms the idea  
776 of the shift of the Polar Front (PF) towards southern latitudes during North Atlantic Heinrich  
777 events. Indeed, Eynaud et al. (2009) proposed a conceptual scheme for the position of the PF on  
778 the western Iberian margin during Heinrich events and its influence on the local hydrology, and  
779 noticed that the protrusion of subpolar waters extended until approximately 40°N. Core MD95-  
780 2042 (37°48'N), at the southern limb of the Ruddiman belt (i.e. between 40 and 55°N;  
781 Ruddiman, 1977), was affected by subpolar waters and iceberg discharges. However, it is  
782 surprising to observe that the peaks of *B. tepikiense* are even larger during GS not associated with  
783 HS on the SW Iberian margin. When considering dinocyst, foraminiferal, and especially  
784 alkenone-based SST reconstructions, HS are characterised by the coldest temperatures (Figs. 3  
785 and 4). We can therefore assume that temperatures were probably too cold during summer  
786 months to permit the expansion of *B. tepikiense*. This hypothesis is reinforced by the large  
787 excursions towards cold summer temperatures observed with dinocyst and foraminiferal SST  
788 reconstructions (Fig. 3). The huge advection of subpolar waters down to the SW Iberian margin  
789 during each GS, and especially HS, is furthermore reinforced by the dinocyst SSS reconstructions  
790 that show a generally more pronounced influence of meltwater in this sector compared with the  
791 westernmost part of the Mediterranean Sea (average salinity offset of around 1 psu between the  
792 sectors; Fig. 3). This is especially true for HS 4, characterised by salinities of around 31 on the  
793 SW Iberian margin and 33 in the Alboran Sea (Fig. 3). We thus show the pronounced impact of  
794 subpolar waters affecting the SW Iberian margin during each GS and especially during HS, while  
795 the Alboran Sea is only impacted by huge freshwater discharges during HS.

796

797 **6.2.3. A first attempt to interpret the dinocyst seasonality signal**

798

799 Sea surface temperatures and precipitation are environmental parameters directly linked to  
800 seasonality in the study region, and the difference between August and February SST estimates  
801 derived from dinocysts may contain important information regarding the seasonality (Fig. 5).  
802 Overall, the two cores show excursions in seasonality reconstructions towards a higher seasonal  
803 contrast during GS due to extremely cold February SST recorded during these cold intervals. At  
804 the SW Iberian margin, seasonal contrasts during GI appear similar to the present-day range,  
805 while extremely pronounced seasonal contrasts of roughly similar magnitude are recorded during  
806 each GS. The pattern of seasonality is very close to the relative abundance curve of *B. tepikiense*  
807 (Fig. 5). In the Alboran Sea, higher seasonal contrasts are mainly noted during HS and also  
808 correspond to higher percentages of *B. tepikiense*. It is not surprising to find parallels between  
809 this species and the seasonal signal since highest abundances of this species are found in areas  
810 today characterised by high-amplitude (10°C) seasonal temperature shifts (Rochon et al., 1999).  
811 In the Alboran Sea, it confirms the establishment of an enhanced seasonal temperature contrast  
812 compared to the present-day caused by a strong decrease in winter SST during HS (Combourieu-  
813 Nebout et al., 2002). At the SW Iberian margin, it reveals very clearly the marked shift between  
814 seasonal temperatures during each GS.

815 In the Alboran Sea, another climatic trend is superimposed on the general observations made  
816 above with, in broad terms, stronger seasonal contrasts during the early part of the record  
817 between 50 and 38 ka, compared to the period 38-31 ka (Fig. 5). Since seasonality and precession  
818 are closely linked, we show the precession curve (Berger and Loutre, 1991) alongside the  
819 reconstruction of seasonality (Fig. 5). It appears that lower seasonal contrasts are observed during

the precession minimum and *vice versa* (Fig. 5). We would have expected higher seasonal contrasts during the precession minimum since this orbital parameter enhanced the Mediterranean climate with warmer summer and wetter winters (Meijer and Tüenter, 2007). When looking at February SST reconstructions in the Alboran Sea, one can note that fluctuations during GS and GI are of similar magnitude (Fig. 5). The contrast is mainly due to August SST reconstructions that show colder values between HS 4 and HS 3 than between HS 5 and HS 4. Our data would suggest a link between the Alboran Sea paleohydrology and the precession signal through a climatic forcing acting on August temperatures. A first hypothesis could involve the general strengthening of the gyre-induced upwelling in the Alboran Sea during the time interval 38-31 ka favouring a cooling of sea-surface waters compared to the period 50-38 ka. However, the functioning of the gyres is mainly controlled today by winter conditions. Furthermore, no large differences are observed between 50-38 ka and 38-31 ka in terms of total dinocyst concentrations and heterotrophic dinocyst species, these latter proxies indicating paleoproductivity conditions probably connected to gyre-induced upwelling intensity. Greater stratification of the Alboran water column may also be suggested for the period 50-38 ka compared to the period 38-31 ka on the basis of the observation of dinocyst and foraminiferal August/summer SST (Fig. 3). Indeed, SSTs in August and summer are similar between 38 and 31 ka and are more distinct between 50 and 38 ka (Fig. 3). This might suggest a greater stratification of water masses during summers within the interval 50-38 ka and a stronger mixing of water masses during summers within the interval 38-31 ka. Warmer dinocyst SSTs might relate to sea-surface conditions while foraminiferal SSTs would incorporate SST signals at greater depths in the water column for the period 50-38 ka. Further investigation will be necessary to verify and explore on longer time-scales: a) the imprint of precession on the seasonality changes inferred from dinocysts, and b) the functioning of the mesoscale energetic features in the Alboran Sea represented by two

844 anticyclonic gyres today.



## 7. CONCLUSION

We have characterised glacial climate variability between 25 and 50 ka BP by comparing surface paleohydrology signals on both sides of the Strait of Gibraltar (Alboran Sea and SW Iberian margin). Comparison of dinocyst assemblages enables the reconstruction of hydrological features at both locations and we present, in this study, the first quantitative dinocyst reconstructions (SST and SSS) for MIS 3 obtained at mid-latitudes. Our hydrological quantifications acquired for both cores reproduce millennial-scale changes correlated to the D-O climatic variability, with a pattern of marked decrease in SST accompanied by a strong freshening of sea-surface waters evident during each GS on the SW Iberian margin and during HS in the Alboran Sea. Furthermore, we show similar patterns and amplitudes in SST reconstructions based on dinocysts, foraminifera and alkenones, and in SSS derived from dinocysts and foraminiferal SST coupled with planktonic  $\delta^{18}\text{O}$ . Larger discrepancies between dinocyst and foraminiferal estimates occur for summer reconstructions than for winter reconstructions, which are very similar in amplitude. We furthermore show the occurrence of cold taxa (including *B. tepikiense* and *S. elongatus*) during GS and the presence of thermophilous ones (*S. mirabilis* and *Impagidinium* spp.) during GI. However, the amplitude of variation in these taxa is not equivalent at both sites. *B. tepikiense* characterises each GS in the SW Iberian margin while it only develops during HS in the Alboran Sea. This pattern reflects, in the Alboran Sea, the maximum climatic deterioration during HS and the incursion of low-salinity subpolar waters to the western Mediterranean. During other GS (i.e. excluding HS), conditions were less severe in the Alboran Sea as is reflected by the occurrence of *O. centrocarpum* at very high relative abundances in the Alboran Sea and low values on the SW Iberian margin. This species conceivably reflects the inflow of cool North Atlantic waters to the

868 western Mediterranean, synchronously with stronger deep convection occurring at that time in the  
869 western Mediterranean. Finally, expansions of temperate to tropical taxa testify to the installation  
870 of warm sea-surface waters during GI. In the Alboran Sea, a high primary productivity pattern is  
871 deduced from heterotrophic species and high total dinocyst concentrations, suggesting gyre-  
872 induced upwelling due to prevailing southward-shifted westerlies above the Mediterranean at that  
873 time. The functioning of the gyre on multi-millennial timescales has also been discussed in light  
874 of seasonality reconstructions based on dinocysts. However, the relationships between gyre  
875 dynamics, seasonality and precession need to be explored in longer records covering several  
876 precession cycles. The dinocyst data thus exhibit regional trends and suggest distinct oscillations  
877 of sea-surface temperature and salinity, documenting the combined influence of atmospheric and  
878 hydrologic processes impacting on the western Mediterranean Sea and eastern subtropical  
879 latitudes of the North Atlantic during the abrupt climatic events of MIS 3.

## 8. Acknowledgements

Thanks to the French polar institute IPEV (*Institut Paul Emile Victor*), the captain and the crew of the Marion Dufresne and the scientific team of the 1995 IMAGES cruise. We wish to thank Mr. Y. Balut for his assistance at sea and M. Castera and O. Ther for invaluable technical assistance at the laboratory. We gratefully acknowledge the reviewers, whose comments have enabled us to greatly improve this manuscript. We thank W. Fletcher for improving the English language of the manuscript. This study was supported by the French CNRS and contributes to the EuroCLIMATE project RESOLuTION.

## 9. References

- Abrantes, F., 2000. 200 000 yr diatom records from Atlantic upwelling sites reveal maximum productivity during LGM and a shift in phytoplankton community structure at 185 000 yr. *Earth and Planetary Science Letters* 176(1), 7-16.
- Ambar, I., Serra, N., Brogueira, M.J., Cabecadas, G., Abrantes, F., Freitas, P., Goncalves, C., Gonzalez, N., 2002. Physical, chemical and sedimentological aspects of the Mediterranean outflow off Iberia. *Deep-Sea Research II* 49, 4163-4177.
- Aristegui, J., Alvarez-Salgado, X.A., Barton, E.D., Figueiras, F.G., Hernandez-Leon, S., Roy, C., Santos, A.M.P., 2005. Chapter 23 : oceanography and fisheries of the Canary current/Iberian region of the eastern North Atlantic (18a,E). In : Brink K.H. (ed.), Robinson A.R. (ed.) *The sea :*

- 903 the global coastal ocean : interdisciplinary regional studies and syntheses. Harvard : Harvard  
904 University Press, 877-931.
- 905
- 906 Baldacci, A., Corsini, G., Grasso, R., Manzella, G., Allen, J.T., Cipollini, P., Guymer, T.H.,  
907 Sanith, H.M., 2001. A study of the Alboran sea mesoscale system by means of empirical  
908 orthogonal function decomposition of satellite data. *Journal of Marine Systems* 29, 293-311.
- 909
- 910 Bard, E., Rostek, R., Turon, J.L., Gendreau, S., 2000. Hydrological impact of Heinrich events in  
911 the subtropical northeast Atlantic. *Science* 289, 1321-1324.
- 912
- 913 Bard, E., Rostek, F., M  not-Combes, G., 2004. Radiocarbon calibration beyond 20,000 14C yr  
914 B.P. by means of planktonic foraminifera of the Iberian Margin. *Quat. Res.* 61, 204-214.
- 915
- 916 Bassinot, F., Labeyrie, L., 1996. IMAGES MD 101, a coring cruise of the R/V Marion Dufresne  
917 in the North Atlantic and Norwegian Sea. *Institut Fran  ais pour la Recherche et la Technologie*  
918 *Polaires, Plouzan  *, pp. 217.
- 919
- 920 Benzohra, M., Millot, C., 1995. Characteristics and circulation of the surface and intermediate  
921 water masses off Algeria. *Deep-Sea Research I* 42 (10), 1803-1830.
- 922
- 923 Berger, A., Loutre, M.F., 1991. Insolation values for the climate of the last 10 million years.  
924 *Quaternary Science Reviews* 10 (4), 297-317.
- 925

- 926 Béthoux, J.P., 1979. Budgets of the Mediterranean Sea. Their dependence on the local climate  
927 and on the characteristics of the Atlantic waters. *Oceanol. Acta* 2, 157-163.  
928
- 929 Béthoux, J. P., 1984. Paléo-hydrologie de la Mer Méditerranée au cours des derniers 20 000 ans.  
930 *Oceanologica Acta* 7, 43-48.  
931
- 932 Bigg, G.R., Wadley, M.R., 2001. Millennial-scale variability in the oceans: an ocean modelling  
933 view. *J. Quat. Sci.* 16, 309-319.  
934
- 935 Bigg, G.R., Rohling, E.J., 2000. An oxygen isotope dataset for marine waters. *Journal of*  
936 *Geophysical Research* 105, 8527-8535.  
937
- 938 Bond, G., Heinrich, H., Broecker, W., Labeyrie, L., McManus, J., Andrews, J., Huon, S.,  
939 Jantschik, R., Clasen, S., Simet, C., Tedesco, C., Klas, M., Bonani, G., Ivy, S., 1992. Evidence  
940 for massive discharges of icebergs into the North Atlantic ocean during the last glacial period.  
941 *Nature* 360, 245-249.  
942
- 943 Bond, G., Broecker, W., Johnsen, S., McManus, J., Labeyrie, L., Jouzel, J., Bonani, G., 1993.  
944 Correlations between climate records from North Atlantic sediments and Greenland ice. *Nature*  
945 365, 143-147.  
946
- 947 Bormans, M., Garret, C., 1989. A simple criterion for gyre formation by the surface outflow from  
948 a strait, with application to the Alboran Sea. *Journal of Geophysical Research* 94 (C9), 12637-  
949 12644.

- 950
- 951 Bouimetarhan, I., Marret, F., Dupont, L., Zonneveld, K., 2009. Dinoflagellate cyst distribution in  
952 marine surface sediments off West Africa (6-17°N) in relation to sea-surface conditions,  
953 freshwater input and seasonal coastal upwelling. *Marine Micropaleontology* 71, 113-130.  
954
- 955 Bout-Roumazielles, V., Combourieu Nebout, N., Peyron, O., Cortijo, E., Landais, A., Masson-  
956 Delmotte, V., 2007. Connection between South Mediterranean climate and North African  
957 atmospheric circulation during the last 50,000 yr BP North Atlantic cold events. *Quaternary*  
958 *Science Reviews* 26 (25-28), 3197-3215.  
959
- 960 Bradford, M.R., Wall, D.A., 1984. The distribution of Recent organic walled dinoflagellate cysts  
961 in the Persian Gulf, Gulf of Oman, and north-western Arabian Sea. *Palaeontographica* 192(B), 1-  
962 84.  
963
- 964 Broecker, W.S., 2006. Abrupt climate change revisited. *Global and Planetary Change* 54, 211-  
965 215.  
966
- 967 Cacho, I., Grimalt, J.O., Pelejero, C., Canals, M., Sierro, F.J., Flores, J.A., Shackleton, N.J.,  
968 1999. Dansgaard-Oeschger and Heinrich event imprints in Alboran Sea paleotemperatures.  
969 *Paleoceanography* 14(6), 698-705.  
970
- 971 Cacho, I., Grimalt, J.O., Sierro, F.J., Shackleton, N.J., Canals, M., 2000. Evidence for enhanced  
972 Mediterranean thermohaline circulation during rapid climatic coolings. *Earth and Planetary*  
973 *Science Letters* 183(3-4), 417-429.

- 974
- 975 Cacho, I., Shackleton, N., Elderfield, H., Sierro, F.J., Grimalt, J.O., 2006. Glacial rapid  
976 variability in deep-water temperature and  $\delta^{18}\text{O}$  from the Western Mediterranean Sea. *Quaternary*  
977 *Science Reviews* 25 (23-24), 3294-3311.
- 978
- 979 Candela, J., Winant, C., Bryden, H., 1989. Meteorologically forced subinertial flows through the  
980 Strait of Gibraltar. *Journal of Geophysical Research* 94 (C9), 12667-12679.
- 981
- 982 Cayre, O., Lancelot, Y., Vincent, E., 1999. Paleoceanographic reconstructions from planktonic  
983 foraminifera off the Iberian Margin: Temperature, salinity, and Heinrich events.  
984 *Paleoceanography* 14(3), 384-396.
- 985
- 986 Clement, A.C., Peterson, L., 2008. Mechanisms of abrupt climate change of the last glacial  
987 period. *Reviews of Geophysics* 46, RG4002, 1-39.
- 988
- 989 Combourieu-Nebout, N., Paterne, M., Turon, J.L., Siani, G., 1998. A high resolution record of  
990 the last deglaciation in the central Mediterranean Sea : palaeovegetation and palaeohydrological  
991 evolution. *Quaternary Science Reviews* 17, 303-317.
- 992
- 993 Combourieu-Nebout, N., Turon, J.L., Zahn, R., Capotondi, L., Londeix, L., Pahnke, K., 2002.  
994 Enhanced aridity and atmospheric high-pressure stability over the western Mediterranean during  
995 the North Atlantic cold events of the past 50 k.y. *Geology* 30, 863-866.
- 996

- 997 Craig, H., Gordon, L.I., 1965. Stable isotopes in Oceanographic Studies and Paleotemperatures.  
998 (Tongiorgi eds, CNR Pisa, 1965).  
999
- 1000 Dale, B., 1977. New observations on *Peridinium faeroense* Paulsen (1905), and classification of  
1001 small orthoperidinoid dinoflagellates. *British Phycological Journal* 12, 241-253.  
1002
- 1003 Dale, B., 1985. Dinoflagellate cyst analysis of Upper Quaternary sediments in core GIK 15530-4  
1004 from the Skagerrak. *Norsk geologisk tidsskrift* 65, 97-102.  
1005
- 1006 Dale, B., Thorsen, T.A., Fjellså, A., 1999. Dinoflagellate cysts as indicator of cultural  
1007 eutrophication in the Oslofjord, Norway. *Estuarine, Coastal and Shelf Science* 48, 371-382.  
1008
- 1009 Daniaux, A.L., Sánchez-Goñi, M.F., Beaufort, L., Laggoun-Défarge, F., Loutre, M.F., Duprat, J.,  
1010 2007. Dansgaard-Oeschger climatic variability revealed by fire emissions in south-western Iberia.  
1011 *Quat. Sci. Rev.* 26, 1369-1383.  
1012
- 1013 Dansgaard, W., Johnsen, S.J., Clausen, H.B., Dahl-Jensen, D., Gundestrup, N.S., Hammer, C.U.,  
1014 Hvidberg, C.S., Steffenson, J.P., Sveinbjörnsdottir, A.E., Jouzel, J., Bond, G., 1993. Evidence for  
1015 general instability of past climate from a 250-kyr ice-core record. *Nature* 364, 218-220.  
1016
- 1017 de Abreu, L., Shackleton, N.J., Schönfeld, J., Hall, M., Chapman, M., 2003. Millennial-scale  
1018 oceanic climate variability off the western Iberian margin during the last two glacial periods.  
1019 *Marine Geology* 196, 1-20.  
1020



1021 Denton, G.H., Alley, R.B., Comer, G.C., Broecker, W.S., 2005. The role of seasonality in abrupt  
1022 climate change. *Quaternary Science Reviews* 24 (10-11), 1159-1182.

1023  
1024 de Vernal, A., Rochon, A., Turon, J.L., Matthiessen, J., 1997. Organic-walled dinoflagellate  
1025 cysts: palynological tracers of sea-surface conditions in middle to high latitude marine  
1026 environments. *GEOBIOS* 30, 905-920.

1027  
1028 de Vernal, A., Henry, M., Bilodeau, G., 1999. Technique de préparation et d'analyse en  
1029 micropaléontologie. *Les Cahiers du GEOTOP* vol. 3, Université du Québec à Montréal,  
1030 Montréal, Canada.

1031  
1032 de Vernal, A., Henry, M., Matthiessen, J., Mudie, P.J., Rochon, A., Boessenkool, K.P., Eynaud,  
1033 F., Grøsfjeld, K., Guiot, J., Hamel, D., Harland, R., Head, M.J., Kunz-Pirrung, M., Levac, E.,  
1034 Loucheur, V., Peyron, O., Pospelova, V., Radi, T., Turon, J.L., Voronina, E., 2001.

1035 Dinoflagellate cyst assemblages as tracers of sea-surface conditions in the Northern North  
1036 Atlantic, Arctic and sub-Arctic seas: The new 'n = 677' data base and its application for  
1037 quantitative palaeoceanographic reconstruction. *Journal of Quaternary Sciences* 16, 681-698.

1038  
1039 de Vernal, A., Eynaud, F., Henry, M., Hillaire-Marcel, C., Londeix, L., Mangin, S., Matthiessen,  
1040 J., Marret, F., Radi, T., Rochon, A., Solignac, S., Turon, J.L., 2005. Reconstruction of sea-surface  
1041 conditions at middle to high latitudes of the Northern Hemisphere during the last glacial  
1042 maximum (LGM) based on dinoflagellate cyst assemblages. *Quat. Sci. Rev.* 24, 897-924.

1043

- 1044 de Vernal, A., Marret, F., 2007. Organic-walled dinoflagellates : tracers of sea-surface  
1045 conditions, In Hillaire-Marcel and de Vernal (eds.) Proxies in Late Cenozoic Paleoceanography,  
1046 Elsevier, 371-408.
- 1047
- 1048 Devillers, R., de Vernal, A., 2000. Distribution of dinoflagellate cysts in surface sediments of the  
1049 northern North Atlantic in relation to nutrient content and productivity in surface waters. *Marine*  
1050 *Geology* 166, 103-124.
- 1051
- 1052 Dodge, J.D., Harland, R., 1991. The distribution of planktonic dinoflagellates and their cysts in  
1053 the eastern and north-eastern Atlantic Ocean. *New Phytol.* 118, 593-603.
- 1054
- 1055 Duplessy, J.C., Labeyrie, L., Juillet-Leclerc, A., Maitre, F., Duprat, J., Sarnthein, M., 1991.  
1056 Surface salinity reconstruction of the North Atlantic Ocean during the last glacial maximum.  
1057 *Oceanologica Acta* 14, 311-324.
- 1058
- 1059 Elliot, M., Labeyrie, L., Duplessy, J.C., 2002. Changes in North Atlantic deep-water formation  
1060 associated with the Dansgaard-Oeschger temperature oscillations (60–10 ka). *Quat. Sci. Rev.* 21,  
1061 1153-1165.
- 1062
- 1063 Epstein, S., Buchsbaum, R., Lowenstam, H.A., Urey, H.C., 1953. Revised carbonate-water  
1064 isotopic temperature scale. *Geological Society of America Bulletin* 64, 1315-1325.
- 1065

- 1066 Eynaud, F., 1999. Kystes de Dinoflagellés et Evolution paléoclimatique et paléohydrologique de  
1067 l'Atlantique Nord au cours du Dernier Cycle Climatique du Quaternaire. PhD, Bordeaux 1 Univ.,  
1068 291 pp.  
1069
- 1070 Eynaud, F., Turon, J.L., Sánchez-Goñi, M.F., Gendreau, S., 2000. Dinoflagellate cyst evidence of  
1071 “Heinrich-like events” off Portugal during the marine isotopic stage 5. *Mar. Micropal.* 40, 9-21.  
1072
- 1073 Eynaud, F., Turon, J.L., Duprat, J., 2004. Comparison of the Holocene and Eemian  
1074 palaeoenvironments in the South-Icelandic basin: dinoflagellate cysts as proxies for the North  
1075 Atlantic surface circulation. *Review of Paleobotany and Palynology* 128, 55-79.  
1076
- 1077 Eynaud, F., de Abreu, L., Voelker, A., Schönfeld, J., Salgueiro, E., Turon, J.L., Penaud, A.,  
1078 Toucanne, S., Naughton, F., Sánchez-Goñi, M.F., Malaizé, B., Cacho, I., 2009. Position of the  
1079 Polar Front along the western Iberian margin during key cold episodes of the last 45 ka.  
1080 *Geochem. Geophys. Geosyst.* 10, Q07U05, doi:10.1029/2009GC002398.  
1081
- 1082 Eynaud, F., Malaizé, B., de Vernal, A., Zaragosi, S., Pujol, C., Turon, J.L., Cortijo, E., Penaud,  
1083 A., Toucanne, S., Grousset, F.E., submitted for publication. Late Pleistocene (35-10 ka) salinity  
1084 changes along the Celtic margin, eastern North Atlantic.  
1085
- 1086 Fensome, R.A., MacRae, R.A., Williams, G.L., 1998. DINOFLAJ. Geological Survey of Canada  
1087 Open File, 3653.  
1088

- 1089 Fensome, R.A., Williams, G.L., 2004. The Lentin and Williams index of fossil dinoflagellates,  
1090 2004 edition. AASP Foundation Contributions Series, 42, 909 pp.  
1091
- 1092 Fiúza, A.F.G., 1984. Hidrologia e dinâmica das águas costeiras de Portugal. Ph.D. thesis, Univ.  
1093 of Lisbon, Lisbon.  
1094
- 1095 Fiúza, A.F.G., Hamann, M., Ambar, I., Del Rio, G.D., González, N., Cabanas, J.M., 1998. Water  
1096 masses and their circulation off western Iberia during May 1993. Deep Sea Res. I 45, 1127-1160.  
1097
- 1098 Fletcher, W.J., Sánchez-Goñi M.F., 2008. Orbital- and sub-orbital scale climate impacts on  
1099 vegetation of the western Mediterranean basin over the last 48,000 yr. Quat. Res. 70, 451-464.  
1100
- 1101 Frigola, J., Moreno, A., Cacho, I., Canals, M., Sierro, F.J., Flores, J.A., Grimalt, J.O., 2008.  
1102 Evidence of abrupt changes in Western Mediterranean Deep Water circulation during the last 50  
1103 kyr: A high-resolution marine record from the Balearic Sea. Quaternary International 181 (1), 88-  
1104 104.  
1105
- 1106 Garcia-Gorriz, E., Carr, M.E., 1999. The climatological annual cycle of satellite-derived  
1107 phytoplankton pigments in the Alboran Sea. Geophysical Research Letters 26 (19), 2985-2988.  
1108
- 1109 Garcia-Lafuente, J., Cano, N., Vargas, M., Rubin, J.P., Hernandez-Guerra, A., 1998. Evolution of  
1110 the Alboran Sea hydrographic structures during July 1993. Deep Sea Research I 45, 39-65.  
1111

- 1112 Garcia-Lafuente, J., Delgado, J., Vargas, J.M., Vargas, M., Plaza, F., Sarhan, T., 2002. Low  
1113 frequency variability of the exchanged flows through the Strait of Gibraltar during CANIGO.  
1114 Deep-Sea Research II 49 (19), 4051-4067.  
1115
- 1116 Garcia-Soto, C., Pingree, R.D., Valdés, L., 2002. Navidad development in the southern Bay of  
1117 Biscay: Climate change and swoddy structure from remote sensing and in situ measurements. J.  
1118 Geophys. Res. 107 (C8), 3118.  
1119
- 1120 Grootes, P.M., Stuiver, M., White, J.W.C., Johnsen, S., Jouzel, J., 1993. Comparison of oxygen  
1121 isotope records from the GISP2 and GRIP Greenland ice cores. Nature 366, 552-554.  
1122
- 1123 Grøsfjeld, K., Funder, S., Seidenkrantz, M.S., Glaister, C., 2006. Last Interglacial marine  
1124 environments in the White Sea region, north-western Russia. Boreas 35(3), 493-520.  
1125
- 1126 Guiot, J., Goeury, C., 1996. PPPbase, a software for statistical analysis of paleoecological data.  
1127 Dendrochronologia 14, 295-300.  
1128
- 1129 Guiot, J., de Vernal, A., 2007. Transfer functions: methods for quantitative paleoceanography  
1130 based on microfossils. In Hillaire-Marcel and de Vernal (eds.). Proxies in Late Cenozoic  
1131 Paleoceanography, Elsevier, 523-563.  
1132
- 1133 Harland, R., 1983. Distribution maps of Recent dinoflagellate cysts in bottom sediments from the  
1134 North Atlantic Ocean and adjacent seas. Paleontology 26(2), 321-387.  
1135

- 1136 Harland, R., Nordberg, K., Filipsson, H.L., 2004a. A high-resolution dinoflagellate cyst record  
1137 from latest Holocene sediments in Koljö Fjord, Sweden. *Review of Palaeobotany and Palynology*  
1138 128, 119-141.  
1139
- 1140 Harland, R., Nordberg, K., Filipsson, H.L., 2004b. The seasonal occurrence of dinoflagellate  
1141 cysts in surface sediments from Koljö Fjord, west coast of Sweden - a note. *Review of*  
1142 *Palaeobotany and Palynology* 128, 107-117.  
1143
- 1144 Hayes, A., Kucera, M., Kallel, N., Saffi L., Rohling, E. J., 2005. Glacial Mediterranean sea  
1145 surface temperatures based on planktonic foraminiferal assemblages. *Quaternary Science*  
1146 *Reviews* 24, 999-1 016.  
1147
- 1148 Head, M.J., 1996. Modern dinoflagellate cysts and their biological affinities. In “*Palynology:*  
1149 *principles and Applications. Chapter 30.*” (Jansonius, J., and McGregor, D.C., editors), AASP  
1150 *Foundation*, 1 197-1 248.  
1151
- 1152 Hemming, S.R., 2004. Heinrich events: Massive late Pleistocene detritus layers of the North  
1153 Atlantic and their global climate imprint, *Rev. Geophys.*, 42, RG1005,  
1154 doi:10.1029/2003RG000128.  
1155
- 1156 Hill, A.E., Mitchelson-Jacob, E.G., 1993. Observations of a poleward-flowing saline core on the  
1157 continental slope west of Scotland. *Deep-Sea Research* 40, 1521-1527.  
1158

- 1159 Holzwarth, U., Meggers, H., Esper, O., Kuhlmann, H., Freudenthal, T., Hensen, C., Zonneveld,  
1160 K.A.F., 2010. NW African climate variations during the last 47,000 years: Evidence from  
1161 organic-walled dinoflagellate cysts. *Palaeogeography, Palaeoclimatology, Palaeoecology* 291 (3-  
1162 4), 443-455.
- 1163
- 1164 Hurrell, J.W., 1995. Decadal trends in the North Atlantic Oscillation: Regional temperatures and  
1165 precipitation. *Science* 269, 676-679.
- 1166
- 1167 Iorga, M., Lozier, M.S., 1999. Signature of the Mediterranean outflow from a North Atlantic  
1168 climatology: 1. Salinity and density field. *J. Geophys. Res.* 104 (C11), 25 985-26 009.
- 1169
- 1170 Johnsen, S.J., Clausen, H.B., Dansgaard, W., Fuhrer, K., Gundestrup, N., Hammer, C.U., Iversen,  
1171 P., Jouzel, J., Stauffer, B., Steffensen, J.P., 1992. Irregular glacial interstadial recorded in a new  
1172 Greenland ice core. *Nature* 359(6393), 311-313.
- 1173
- 1174 Johnson, R.G., 1997. Ice age initiation by an ocean-atmospheric circulation change in the  
1175 Labrador Sea. *Earth and Planetary Science Letters* 148 (1-2), 367-379.
- 1176
- 1177 Kageyama, M., Mignot, J., Swingedouw, D., Marzin, C., Alkama, R., Marti, O., 2009. Glacial  
1178 climate sensitivity to different states of the Atlantic Meridional Overturning Circulation: results  
1179 from the IPSL model. *Climate of the Past* 5, 551-570.
- 1180
- 1181 Keigwin, L. D., Boyle, E.A., 1999. Surface and deep ocean variability in the northern Sargasso  
1182 Sea during marine isotope stage 3. *Paleoceanography* 14(2), 164-170.

1183

1184 Kodrans-Nsiah, M., de Lange, G.J., Zonneveld, K.A.F., 2008. A natural exposure experiment on  
1185 short-term species-selective aerobic degradation of dinoflagellate cysts. *Review of Palaeobotany*  
1186 *and Palynology* 152 (1-2), 32-39.

1187

1188 Kucera, M., Weinelt, M., Kiefer, T., Pflaumann, U., Hayes, A., Weinelt, M., Chen, M.T., Mix,  
1189 A.C., Barrows, T.T., Cortijo, E., Duprat, J., Juggins, S., Waelbroeck, C., 2005. Reconstruction of  
1190 sea-surface temperatures from assemblages of planktonic foraminifera: Multi-technique approach  
1191 based on geographically constrained calibration data sets and its application to glacial Atlantic  
1192 and Pacific Oceans. *Quaternary Science Reviews* 24(7-9), Special Issue, 951-998.

1193

1194 Kucera, M., 2007. Planktonic foraminifera as tracers of past oceanic environments. In: Hillaire-  
1195 Marcel, C. and de Vernal, A. (eds): *Developments in Marine Geology, Volume 1, Proxies in late*  
1196 *Cenozoic Paleoceanography*, Elsevier, 213-262.

1197

1198 Lebreiro, S.M., Moreno, J.C., Abrantes, F.F., Pflaumann, U., 1997. Productivity and  
1199 paleoceanographic implications on the Tore Seamount (Iberian Margin) during the last 225 kyr:  
1200 Foraminiferal evidence. *Paleoceanography* 12(5), 718-727.

1201

1202 LeGrande, A., Schmidt, G.A., 2006. Global gridded data set of the oxygen isotopic composition  
1203 in seawater. *Geophysical Research Letters* 33, L12604. doi:10.1029/2006GL026011.

1204

1205 Lewis, J., 1988. Cysts and sediments: *Gonyaulax polyedra* (*Lingulodinium machaerophorum*) in  
1206 Loch Ceran. *Journal of the Marine Biology Association of the United Kingdom* 68, 701-714.



- 1207
- 1208 Macias, D., Navarro, G., Echevarria, F., Garcia, C.M., Cueto, J.L., 2007. Phytoplankton  
1209 distribution in the north-western Alboran Sea and meteorological forcing: a remote sensing study.  
1210 Journal of Marine Research 64 (4), 523-543.
- 1211
- 1212 Macias, D., Bruno, M., Echevarria, F., Vazquez, A., Garcia, C.M., 2008. Meteorologically-  
1213 induced mesoscale variability of the North-western Alboran Sea (southern Spain) and related  
1214 biological patterns. Estuarine, Coastal and Shelf Science 78, 250-266.
- 1215
- 1216 Malaizé, B., Caley, T., 2009. Sea surface salinity reconstructions as seen with foraminifera shells:  
1217 Methods and cases studies. European Physical journal 167, Special Topics, 179-190.
- 1218
- 1219 Mangin, S., 2002. Distribution actuelle des kystes de dinoflagellés en Méditerranée occidentale et  
1220 application aux fonctions de transfert, vol. 1. Memoir of DEA, University of Bordeaux, 34 pp.
- 1221
- 1222 MARGO Project Members, 2009. Constraints on the magnitude and patterns of ocean cooling at  
1223 the Last Glacial Maximum. Nature Geoscience 2, 127-132.
- 1224
- 1225 Marret, F., 1994. Distribution of dinoflagellate cysts in recent marine sediments from the east  
1226 Equatorial Atlantic (Gulf of Guinea). Review of Palaeobotany and Palynology 84, 1-22.
- 1227
- 1228 Marret, F., Turon, J.L., 1994. Paleohydrology and paleoclimatology off Northwest Africa during  
1229 the last glacial-interglacial transition and the Holocene : Palynological evidences. Marine  
1230 Geology 118, 107-117.

- 1231
- 1232 Marret, F., Zonneveld, K.A.F., 2003. Atlas of modern organic-walled dinoflagellate cyst  
1233 distribution. *Review of Palaeobotany and Palynology* 125, 1-200.
- 1234
- 1235 Marret, F., Eiríksson, J., Knudsen, K.L., Turon, J.L., Scourse, J.D., 2004. Distribution of  
1236 dinoflagellate cyst assemblages in surface sediments from the northern and western shelf of  
1237 Iceland. *Review of Palaeobotany and Palynology* 128, 35-53.
- 1238
- 1239 Martrat, B., Grimalt, J.O., Lopez-Martinez, C., Cacho, I., Sierro, F.J., Flores, J.A., Zahn, R.,  
1240 Canals, M., Curtis, J.H., Hodell, D.A., 2004. Abrupt temperature changes in the western  
1241 Mediterranean over the past 250,000 years. *Science* 306, 1762-1765.
- 1242
- 1243 Martrat, B., Grimalt, J.O., Shackleton, N.J., de Abreu, L., Hutterli, M.A., Stocker, T.F., 2007.  
1244 Four climate cycles of recurring deep and surface water destabilizations on the Iberian Margin.  
1245 *Science* 317, 502-507.
- 1246
- 1247 Maslin, M.A., Shackleton, N. J., Pflaumann, U., 1995. Surface water temperature, salinity and  
1248 density changes in the northeast Atlantic during the last 45,000 years: Heinrich events, deep-  
1249 water formation and climate rebounds. *Paleoceanography* 10(3), 527-544.
- 1250
- 1251 Matsuzaki, K.M.R., Eynaud, F., Malaizé, B., Grousset, F.E., Tisserand, A., Rossignol, L.,  
1252 Charlier, K., Jullien, E., 2011. Paleooceanography of the Mauritanian margin during the last two  
1253 climatic cycles: from planktonic foraminifera to African climate dynamic. *Marine*  
1254 *Micropaleontology*, doi:10.1016/j.marmicro.2011.01.004.

- 1255
- 1256 Matthiessen, J., 1995. Distribution patterns of dinoflagellate cysts and other organic-walled  
1257 microfossils in recent Norwegian-Greenland Sea sediments. *Mar. Micropal.* 24, 307-334.  
1258
- 1259 Mauritzen, C., 1996. Production of dense overflow waters feeding the North Atlantic across the  
1260 Greenland-Scotland Ridge. Part 1: Evidence for a revised circulation scheme. *Deep-Sea Research*  
1261 *I* 43(6), 769-806.  
1262
- 1263 Meijer, P.Th., Tuentner, E., 2007. The effect of precession-induced changes in the Mediterranean  
1264 freshwater budget on circulation at shallow and intermediate depth. *Journal of Marine Systems*  
1265 68 (3-4), 349-365.  
1266
- 1267 Mertens, K., Ribeiro, S., et al., 2009. Process length variation in cysts of a dinoflagellate,  
1268 *Lingulodinium machaerophorum*, in surface sediments: Investigating its potential as salinity  
1269 proxy. *Marine Micropaleontology* 70, 54-69.  
1270
- 1271 Moreno, A., Cacho, I., Canals, M., Prins, M.A., Sánchez-Goñi, M.F., Grimalt, J.O., Weltje, G.J.,  
1272 2002. Saharan dust transport and high-latitude glacial climatic variability: The Alboran Sea  
1273 record. *Quaternary Research* 58 (3), 318-328.  
1274
- 1275 Moreno, A., Cacho, I., Canals, M., Grimalt, J.O., Sanchez-Vidal, A., 2004. Millennial-scale  
1276 variability in the productivity signal from the Alboran Sea record, Western Mediterranean Sea.  
1277 *Palaeogeography, Palaeoclimatology, Palaeoecology* 211 (3-4), 205-219.  
1278

- 1279 Moreno, A., Cacho, I., Canals, M., Grimalt, J.O., Sánchez-Goñi, M.F., Shackleton, N.J., Sierro,  
1280 F.J., 2005. Links between marine and atmospheric processes oscillating on a millennial time-  
1281 scale. A multiproxy study of the last 50,000 yr from the Alboran Sea (Western Mediterranean  
1282 Sea). *Quaternary Science Reviews* 24, 1623-1636.
- 1283
- 1284 Morzadec-Kerfourn, M.T., 1988. Distribution des kystes de dinoflagellés dans les sédiments  
1285 Pléistocènes de la marge Guinéenne de l'Afrique (Equamarge I, 1983) = Distribution of  
1286 dinoflagellate cysts in Pleistocene sediments of the Guinean margin of Africa, Equamarge I,  
1287 1983. *Palaeogeography, palaeoclimatology, palaeoecology* 65 (3-4), 201-216.
- 1288
- 1289 Mudie, P.J., 1992. Circum-Arctic Quaternary and Neogene marine palynofloras: paleoecology  
1290 and statistical analysis. In Head, M.J., and Wrenn, J.H. (Eds.), *Neogene and Quaternary*  
1291 *Dinoflagellate Cysts and Acritarchs*. Am. Assoc. Stratigr. Palynol. Foundation, 347-390.
- 1292
- 1293 Mudie, P.J., Rochon, A., Aksu, A.E., Gillespie, H., 2002. Dinoflagellate cysts, freshwater algae  
1294 and fungal spores as salinity indicators in Late Quaternary cores from Marmara and Black seas.  
1295 *Marine Geology* 190, 203-231.
- 1296
- 1297 Mudie, P.J., Rochon, A., Aksu, A.E., Gillespie, H., 2004. Late glacial, Holocene and modern  
1298 dinoflagellate cyst assemblages in the Aegean-Marmara-Black Sea corridor: statistical analysis  
1299 and re-interpretation of the early Holocene Noah's Flood hypothesis. *Review of Palaeobotany*  
1300 *and Palynology* 128, 143-167.
- 1301

- 1302 Naughton, F., Sánchez-Goñi, M.F., Kageyama, M., Bard, E., Duprat, J., Cortijo, E., Desprat, S.,  
1303 Malaizé, B., Joly, C., Rostek, F., 2009. Wet to dry climatic trend in north western Iberia within  
1304 Heinrich events. *Earth Planet. Sci. Lett.* 284(3-4), 329-342.  
1305
- 1306 O'Neill-Baringer, M., Price, J.F., 1999. A review of the physical oceanography of the  
1307 Mediterranean outflow. *Marine Geology* 155, 63-82.  
1308
- 1309 Osborn, T.J., Briffa, K.R., Tett, S.F.B., Jones, P.D., Trigo, R.M., 1999. Evaluation of the North  
1310 Atlantic Oscillation as simulated by a coupled climate model. *Clim. Dyn.* 15, 685-702.  
1311
- 1312 Ostlund, H.G., Craig, H., Broecker, W.S., Spenser, D. (Eds.), 1987. *GEOSECS Atlantic, Pacific*  
1313 *and Indian Ocean Expeditions, vol. 7, Shorebased Data and Graphics, Int. Decade of Ocean*  
1314 *Explor. Natl. Science Found., Washington D.C.*  
1315
- 1316 Pailler, D., Bard, E., 2002. High frequency palaeoceanographic changes during the past 140 000  
1317 yr recorded by the organic matter in sediments of the Iberian Margin. *Palaeogeography,*  
1318 *Palaeoclimatology, Palaeoecology* 181(4), 431-452.  
1319
- 1320 Peliz, A., Dubert, J., Santos, A., Oliveira, P., Le Cann, B., 2005. Winter upper ocean circulation  
1321 in the Western Iberian Basin-Fronts, eddies and poleward flows: An overview. *Deep Sea Res. I*  
1322 52, 621-646.  
1323

- 1324 Penaud, A., Eynaud, F., Turon, J.L., Zaragosi, S., Marret, F., Bourillet, J.F., 2008. Interglacial  
1325 variability (MIS 5 and MIS 7) and dinoflagellate cyst assemblages in the Bay of Biscay (North  
1326 Atlantic). *Marine Micropaleontology* 68, 136-155.  
1327
- 1328 Penaud, A., Eynaud, F., Turon, J.L., Zaragosi, S., Malaizé, B., Toucanne, S., Bourillet, J.F., 2009.  
1329 What forced the collapse of European ice sheets during the last two glacial periods (150 ka B.P.  
1330 and 18 ka cal B.P.)? Palynological evidence. *Palaeogeography, Palaeoclimatology,*  
1331 *Palaeoecology* 281, 66-78.  
1332
- 1333 Penaud, A., Eynaud, F., Turon, J.L., Blamart, D., Rossignol, L., Marret, F., Lopez-Martinez, C.,  
1334 Grimalt, J.O., Malaizé, B., Charlier, K., 2010. Contrasting Heinrich Events 1, 2, and LGM  
1335 conditions off Morocco: Paleoceanographical evidences of warmer LGM and colder HE 1.  
1336 *Quaternary Science Reviews* 29 (15-16), 1923-1939.  
1337
- 1338 Pérez-Folgado, M., Sierro, F.J., Flores, J.A., Cacho, I., Grimalt, J.O., Zahn, R., Shackleton, N.J.,  
1339 2003. Western Mediterranean planktonic foraminifera events and millennial climatic variability  
1340 during the last 70 kyr. *Mar. Micropaleontol.* 48, 49-70.  
1341
- 1342 Pflaumann, U., Duprat, J., Pujol, C., Labeyrie, L.D., 1996. SIMMAX: a modern analogue  
1343 technique to deduce Atlantic sea surface temperatures from planktonic foraminifera in deep-sea  
1344 sediments. *Paleoceanography* 11(1), 15-35.  
1345

- 1346 Raine, R., White, M., Dodge, J.D., 2002. The summer distribution of net plankton dinoflagellates  
1347 and their relation to water movements in the NE Atlantic Ocean, west of Ireland. *Journal of*  
1348 *Plankton Research* 24, 1 131-1 147.
- 1349
- 1350 Reid, P.C., 1972. Dinoflagellate cyst distribution around the British Isles. *J. Mar. Ass. U.K.* 52,  
1351 939-944.
- 1352
- 1353 Reid, P.C., 1974. Gonyaulacacean dinoflagellate cysts from the British Isles. *Nova Hedwigia* 25,  
1354 579-637.
- 1355
- 1356 Relvas, P., Peliz, A., Barton, E.D., da Silva, J.C., Dubert, J., Santos, M., Oliveira, P.B., 2007.  
1357 Western Iberia Upwelling Ecosystem: An oceanographic overview. *Prog. Oceanogr.* 74, 149-173.
- 1358
- 1359 Roche, D., Paillard, D., Cortijo, E., 2004. Constraints on the duration and freshwater release of  
1360 Heinrich event 4 through isotope modelling. *Nature* 432, 379-382.
- 1361
- 1362 Rochon, A., de Vernal, A., Turon, J.L., Matthiessen, J., Head, M.J., 1999. Distribution of Recent  
1363 Dinoflagellate cysts in surface sediments from the North Atlantic Ocean and adjacent seas in  
1364 relation to sea-surface parameters. *Am. Assoc. of Stratigr. Palynol., AASP Contr. Ser.*, 35, 1-152.
- 1365
- 1366 Rogerson, M., Rohling, E.J., Weaver, P.P.E., 2006. Promotion of meridional overturning by  
1367 Mediterranean-derived salt during the last deglaciation. *Paleoceanography* 21, PA4101, 1-8.
- 1368

- 1369 Rohling, E.J., Den Dulk, M., Pujol, C., Vergnaud-Grazzini, C., 1995. Abrupt hydrographic  
1370 change in the Alboran Sea (western Mediterranean) around 8000 yrs BP. *Deep Sea Research I*  
1371 42(9), 1609-1619.
- 1372
- 1373 Rohling, E.J., Abu-Zied, R., Casford, C.S.L., Hayes, A., Hoogakker, B.A.A., 2009. The  
1374 Mediterranean Sea: Present and Past. In: *Physical Geography of the Mediterranean Basin*. Oxford  
1375 Regional Environments. Oxford University Press, Oxford, 592 pp.
- 1376
- 1377 Roucoux, K.H., Tzedakis, P.C., de Abreu, L., Shackleton, N.J., 2005. The response of NW  
1378 Iberian vegetation to North Atlantic climate oscillations during the last 65,000 years. *Quat. Sci.*  
1379 *Rev.* 24, 1637-1653.
- 1380
- 1381 Rouis-Zargouni, I., Turon, J.L., Londeix, L., Essallami, L., Kallel, N., Sicre, M.A., 2010.  
1382 Environmental and climatic changes in the central Mediterranean Sea (Siculo-Tunisian Strait)  
1383 during the last 30 ka based on dinoflagellate cyst and planktonic foraminifera assemblages.  
1384 *Palaeogeography, Palaeoclimatology, Palaeoecology* 285 (1-2), 17-29.
- 1385
- 1386 Ruddiman, W.F., 1977. Late quaternary deposition of ice-rafted sand in the subpolar north  
1387 Atlantic (lat 40° to 65° N). *Geol. Soc. Am. Bull.* 88, 1813-1827.
- 1388
- 1389 Sachs, J. P., Lehman, S.J., 1999. Subtropical North Atlantic temperatures 60,000 to 30,000 years  
1390 ago. *Science* 286, 756-759.
- 1391



- 1392 Sánchez, R.F., Relvas, P., 2003. Spring–summer climatological circulation in the upper layer in  
1393 the region of Cape St.Vincent, southwest Portugal. *ICES J. Mar. Sci.* 60, 1232-1250.  
1394
- 1395 Sánchez Goñi, M.F., Eynaud, F., Turon, J.L., Shackleton, N.J., 1999. High resolution  
1396 palynological record off the Iberian margin: Direct land-sea correlation for the Last Interglacial  
1397 complex. *Earth and Planetary Science Letters* 171 (1), 123-137.  
1398
- 1399 Sánchez-Goñi, M.F., Turon, J.L., Eynaud, F., Gendreau, S., 2000. European climatic response to  
1400 millennial-scale changes in the atmosphere-ocean system during the Last Glacial Period. *Quat.*  
1401 *Res.* 54, 394-403.  
1402
- 1403 Sánchez-Goñi, M.F., Cacho, I., Turon, J.L., Guiot, J., Sierro, F., Peypouquet, J.P., Grimalt, J.O.,  
1404 Shackleton, N.J., 2002. Synchronicity between marine and terrestrial responses to millennial  
1405 scale climatic variability during the last glacial period in the Mediterranean region. *Climate*  
1406 *Dynamics* 19(1), 95-105.  
1407
- 1408 Sánchez-Goñi, M., Landais, A., Fletcher, W., Naughton, F., Desprat, S., Duprat, J., 2008.  
1409 Contrasting impacts of Dansgaard-Oeschger events over a western European latitudinal transect  
1410 modulated by orbital parameters. *Quaternary Science Reviews* 27 (11-12), 1136-1151.  
1411
- 1412 Sánchez-Goñi, M., Landais, A., Cacho, I., Duprat, J., Rossignol, L., 2009. Contrasting  
1413 intrainterstadial climatic evolution between high and middle North Atlantic latitudes: A close-up  
1414 of Greenland Interstadials 8 and 12. *Geochem. Geophys. Geosyst.* 10, Q04U04,  
1415 doi:10.1029/2008GC002369.

- 1416
- 1417 Sánchez-Goñi, M.F., Harrison, S.P., 2010. Millennial-scale climate variability and vegetation  
1418 changes during the Last Glacial: Concepts and terminology. *Quaternary Science Reviews* 29 (21-  
1419 22), 2823-2827.
- 1420
- 1421 Schmidt, G.A., 1999. Error analysis of paleosalinity calculations. *Paleoceanography* 14, 422-429.
- 1422
- 1423 Schulz, M., Berger, W.H., Sarnthein, M., Grootes, P.M., 1999. Amplitude variations of 1470-  
1424 year climate oscillations during the last 100,000 years linked to fluctuations of continental ice  
1425 mass. *Geophysical Research Letters* 26 (22), 3385-3388.
- 1426
- 1427 Serreze, M.C., Carse, F., Barry, R.G., Rogers, J.C., 1997. Icelandic low cyclone activity:  
1428 Climatological features, linkages with the NAO, and relationships with recent changes in the  
1429 Northern Hemisphere circulation. *Journal of Climate* 10, 453-464.
- 1430
- 1431 Shackleton, N.J., Hall, M.A., Vincent, E., 2000. Phase relationships between millennial-scale  
1432 events 64,000-24,000 years ago. *Paleoceanography* 15, 565-569.
- 1433
- 1434 Shackleton, N.J., Fairbanks, R.G., Chiu, T.C., Parrenin, F., 2004. Absolute calibration of the  
1435 Greenland time scale: implications for Antarctic time scales and for  $\delta^{14}\text{C}$ . *Quaternary Science*  
1436 *Reviews* 23, 1513-1522.
- 1437

- 1438 Shackleton, N.J., Opdyke, N.D., 1973. Oxygen isotope and palaeomagnetic stratigraphy of  
1439 equatorial Pacific core V28-238: oxygen isotope temperatures and ice volumes on a  $10^5$  and  $10^6$   
1440 year scale. *Quaternary Research* 3, 39-55.  
1441
- 1442 Sierro, F.J., Hodell, D.A., Curtis, J.H., Flores, J.A., Reguera, I., Colmenero-Hidalgo, E., Barcena,  
1443 M.A., Grimalt, J.O., Cacho, I., Frigola, J., Canals, M., 2005. Impact of iceberg melting on  
1444 Mediterranean thermohaline circulation during Heinrich events. *Paleoceanography* 20, PA2019,  
1445 1-13.  
1446
- 1447 Sprangers, M., Dammers, N., Brinkhuis, H., van Weering, T.C.E., Lotter, A.F., 2004. Modern  
1448 organic-walled dinoflagellate cyst distribution offshore NW Iberia; tracing the upwelling system.  
1449 *Review of Palaeobotany and Palynology* 128, 97-106.  
1450
- 1451 Targarona, J., Warnaar, J., Boessenkool, K.P., Brinkhuis, H., Canals, M., 1999. Recent  
1452 dinoflagellate cyst distribution in the North Canary Basin, NW Africa. *Grana* 38, 170-178.  
1453
- 1454 Thouveny, N., Moreno, E., Delanghe, D., Candon, L., Lancelot, Y., Shackleton, N.J., 2000. Rock  
1455 magnetic detection of distal ice-rafted debris: Clue for the identification of Heinrich layers on the  
1456 Portuguese margin. *Earth Planet. Sci. Lett.* 180, 61-75.  
1457
- 1458 Tintoré, J., La Violette, P.E., Blade, I., Cruzado, A., 1988. A study of an intense density front in  
1459 the eastern Alboran Sea: The Almeria-Oran front. *Journal of Physical Oceanography* 18, 1384-  
1460 1397.  
1461

- 1462 Toucanne, S., Mulder, T., Schönfeld, J., Hanquiez, V., Gonthier, E., Duprat, J., Cremer, M.,  
1463 Zaragosi, S., 2007. Contourites of the Gulf of Cadiz: A high-resolution record of the  
1464 paleocirculation of the Mediterranean outflow water during the last 50,000 years.  
1465 *Palaeogeography, Palaeoclimatology, Palaeoecology* 246(2-4), 354-366.  
1466
- 1467 Turon, J. L., 1984. Le palynoplancton dans l'environnement actuel de l'Atlantique Nord-oriental.  
1468 Evolution climatique et hydrologique depuis le dernier maximum glaciaire. Mémoires de l'Institut  
1469 de Géologie du Bassin d'Aquitaine 17, 313 pp.  
1470
- 1471 Turon, J.L., Londeix, L., 1988. Les assemblages de kystes de dinoflagellés en Méditerranée  
1472 occidentale (Mer d'Alboran): mise en évidence de l'évolution des paléoenvironnement depuis le  
1473 dernier maximum glaciaire. *Bull. Centres Rech. Explor.-prod. Elf-Aquitaine* 12, 313-344.  
1474
- 1475 Turon, J.L., Lézine, A.M., Denèfle, M., 2003. Land-sea correlations for the last glaciation  
1476 inferred from a pollen and dinocyst record from the Portuguese margin. *Quaternary Research* 59,  
1477 88-96.  
1478
- 1479 Viúdez, A., Tintoré, J., 1995. Time and space variability in the eastern Alboran Sea from March  
1480 to May 1990. *J. Geophys. Res.* 100(C5), 8 571-8 586.  
1481
- 1482 Voelker, A.H.L., and Workshop Participants, 2002. Global distribution of centennial-scale  
1483 records for Marine Isotope Stage (MIS) 3: A database. *Quaternary Science Reviews* 21 (10),  
1484 1185-1212.  
1485

- 1486 Voelker, A.H.L., Lebreiro, S.M., Schönfeld, J., Cacho, I., Erlenkeuser, H., Abrantes, F., 2006.  
1487 Mediterranean outflow strengthening during northern hemisphere coolings: A salt source for the  
1488 glacial Atlantic? *Earth and Planetary Science Letters* 245(1-2), 39-55.  
1489
- 1490 Waelbroeck, C., Labeyrie, L., Michel, E., Duplessy, J.C., McManus, J.F., Lambeck, K., Balbon,  
1491 E., Labracherie, M., 2002. Sea-level and deep water temperature changes derived from benthic  
1492 foraminifera isotopic records. *Quaternary Science Reviews* 21 (1-3), 295-305.  
1493
- 1494 Wall, D., Dale, B., Lohmann, G.P., Smith, W.K., 1977. The environment and climatic  
1495 distribution of dinoflagellate cysts in modern marine sediments from regions in the north and  
1496 south Atlantic oceans and adjacent seas. *Mar. Micropaleontol.* 2, 121-200.  
1497
- 1498 Zaragosi, S., Eynaud, F., Pujol, C., Auffret, G.A., Turon, J.L., Garlan, T., 2001. Initiation of  
1499 European deglaciation as recorded in the north-western Bay of Biscay slope environments  
1500 (Meriadzek Terrace and Trevelyan Escarpment): a multi-proxy approach. *Earth Planet. Sci. Lett.*  
1501 188, 493-507.  
1502
- 1503 Zonneveld, K.A.F., Hoek, R.P., Brinkhuis, H., Willems, H., 2001. Geographical distributions of  
1504 organic-walled dinoflagellate cysts in surficial sediments of the Benguela upwelling region and  
1505 their relationship to upper ocean conditions. *Progress in Oceanography* 48, 25-72.

## 10. Figure captions

**Figure 1:** Area of interest with major sea-surface features. The studied cores MD95-2043 (Alboran Sea; 36°8.6'N; 2°37.3'W; 1841 m water depth) and MD95-2042 (Iberian margin; 37°48'N; 10°10'W; 3146 m water depth) are located on the large map, depicting also the bathymetry of the study area and the major surface currents within the Alboran sea; WAG: Western Alboran Gyre; EAG: Eastern Alboran Gyre; AOF: Almeria-Oran Front; AC: Algerian Current. The small map on the left shows large scale North-Atlantic currents with: the North Atlantic Drift (NAD), the Portugal Current (PC) flowing southward from 45°N to 30°N, the Azores Current (AzC) derived from the southern branch of the Gulf Stream and flowing eastward to the Gulf of Cadiz at about 35°N, and the Canary Current (CC) fed by both the AzC and the PC. Together, these currents form the Eastern Boundary Current of the North Atlantic subtropical gyre. A Mediterranean analogue of the dinocyst modern database has been located on the map (M1039). Colors from red to dark blue on the map reflect growing bathymetry towards the deepest areas.

**Figure 2:** MD95-2043 (a) and MD95-2042 (b). Core depths are displayed in centimetres along the vertical axis. The relative abundances of selected dinocyst species are compared with planktonic  $\delta^{18}\text{O}$  data and  $U^{k'}_{37}$ -SST (Core MD95-2043: Cacho et al., 1999; Core MD95-2042: Cayre et al., 1999; Shackleton et al., 2000; Pailler and Bard, 2002), providing the stratigraphical framework for the two cores. Quaternary dinocyst concentrations are also illustrated. HS: Heinrich Stadial; GI: Greenland Interstadial.

**Figure 3:** MD95-2043 (a) and MD95-2042 (b). Quantitative dinocyst reconstructions (February and August SST and SSS, 3PBase-940) compared with SST provided by foraminifera (winter, summer and annual, R-1007) and alkenones ( $U^{k'}_{37}$  - SST), and SSS provided by calculations based on planktonic  $\delta^{18}O$  (*G. bulloides*) and foraminiferal SST estimates (winter and summer, R-1007). Error bars are shown in the figure for the different reconstructions. HS: Heinrich Stadial; GI: Greenland Interstadial.

**Figure 4:** Comparison between cores MD95-2043 and MD95-2042 of a multi-proxy compilation including: selected dinocyst species, total dinocyst concentrations, February dinocyst (3PBase-940) and alkenone SST (Cacho et al., 1999; Pailler and Bard, 2002) reconstructions, percentages of *N. pachyderma* s. (Cacho et al., 1999; Pérez-Folgado et al., 2003), benthic  $\delta^{13}C$  (Cacho et al., 2006), and percentages of the Mediterranean forest (Sánchez-Goñi et al., 2000, 2002; Fletcher and Sánchez-Goñi, 2008). These data are compared with  $\delta^{18}O$  ice core records and the precession signal (Berger and Loutre, 1991). HS: Heinrich Stadial; GI: Greenland Interstadial.

**Figure 5:** MD95-2043 (a) and MD95-2042 (b). Estimation of a parameter of seasonality based on the difference between February and August dinocyst SST reconstructions (3PBase-940), compared with percentages of the dinocyst species *Bitectatodinium tepikiense*, the precession signal (Berger and Loutre, 1991) and planktonic  $\delta^{18}O$  records (*G. bulloides*). Dinocyst and alkenone SST records are also represented, as well as modern SST values. HS: Heinrich Stadial; GI: Greenland Interstadial.

## 11. Appendices

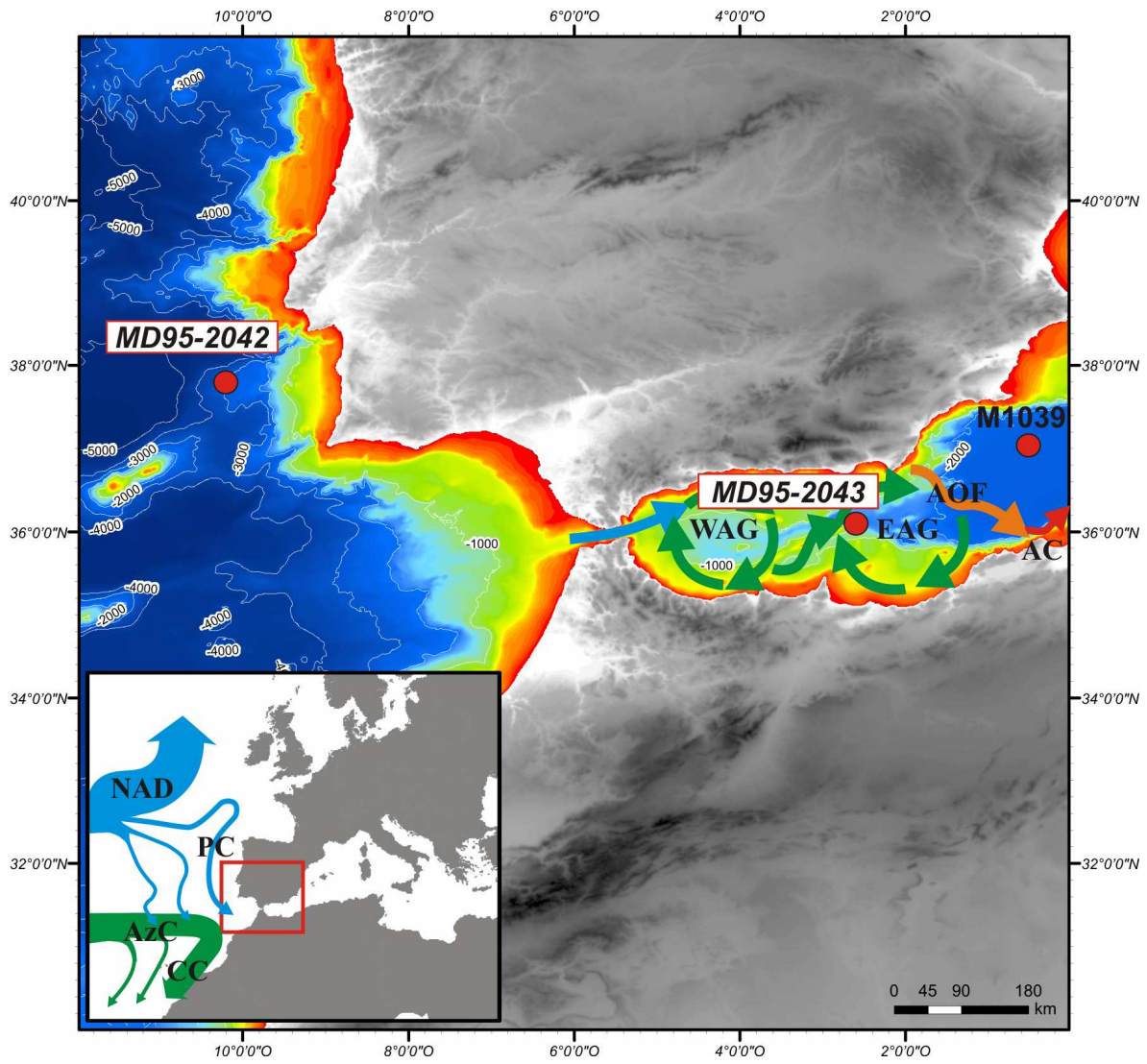
1553 **Appendix A:** MD95-2042 (SW Iberian Margin) and MD95-2043 (Alboran Sea): individual  
1554 counts of dinocyst species, total dinocysts counted and total dinocyst concentrations per sample.

1555  
1556 **Appendix B:** MD95-2042 (SW Iberian Margin) and MD95-2043 (Alboran Sea): lists of the five  
1557 best analogues found with the transfer function 3PBase-940. The geographical coordinates of  
1558 each named analogue can be found on the GEOTOP website  
1559 ([http://www.geotop.ca/index.php?option=com\\_content&task=view&id=762&Itemid=226](http://www.geotop.ca/index.php?option=com_content&task=view&id=762&Itemid=226)). The  
1560 five analogues found by 3PBase-940 have systematically been used for the calculations, the  
1561 threshold (Dmin value of 71.72) may then be considered to judge the good reliability of the  
1562 reconstructed hydrological parameters. The M1039 analogue, highlighted in the tables in bold, is  
1563 a Mediterranean analogue located in Figure 1.

1564



1565



1566

1567

1568

1569 **Figure 1**

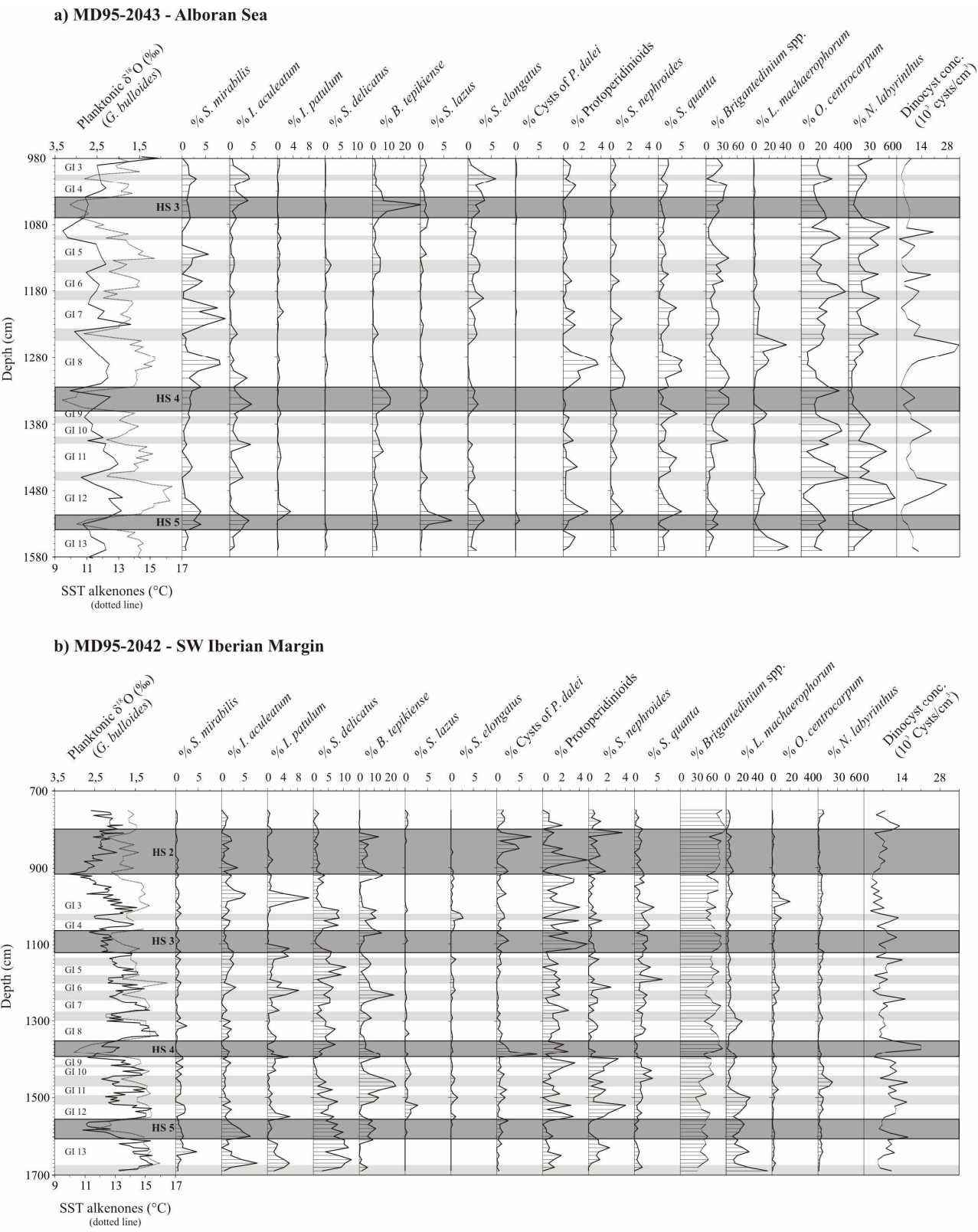
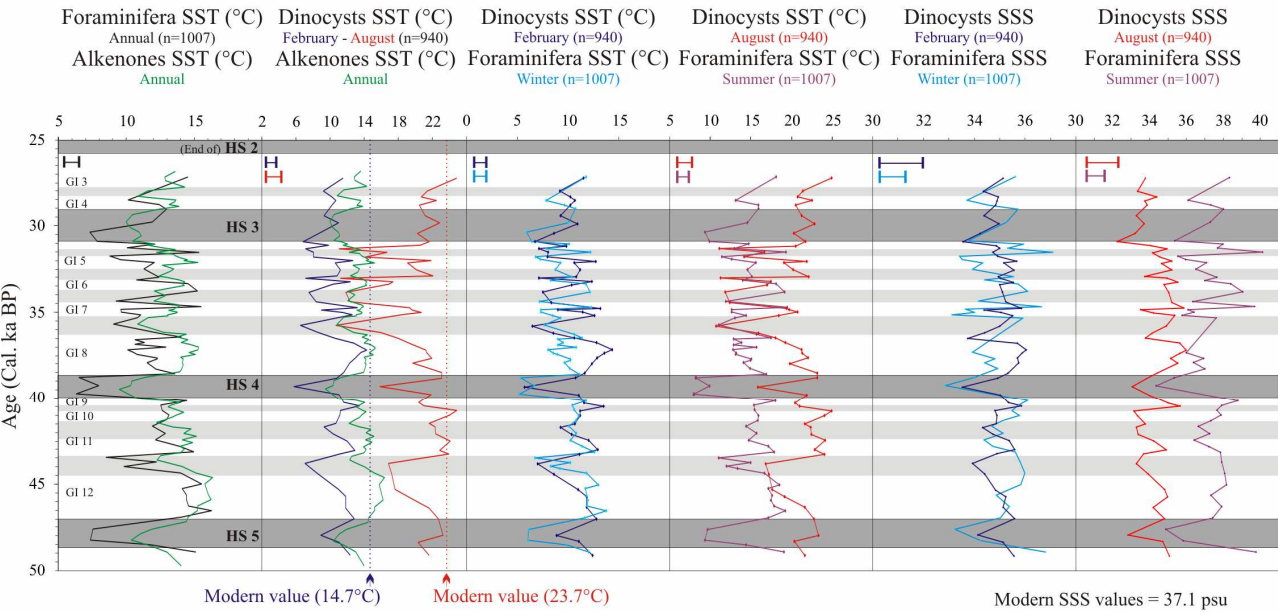
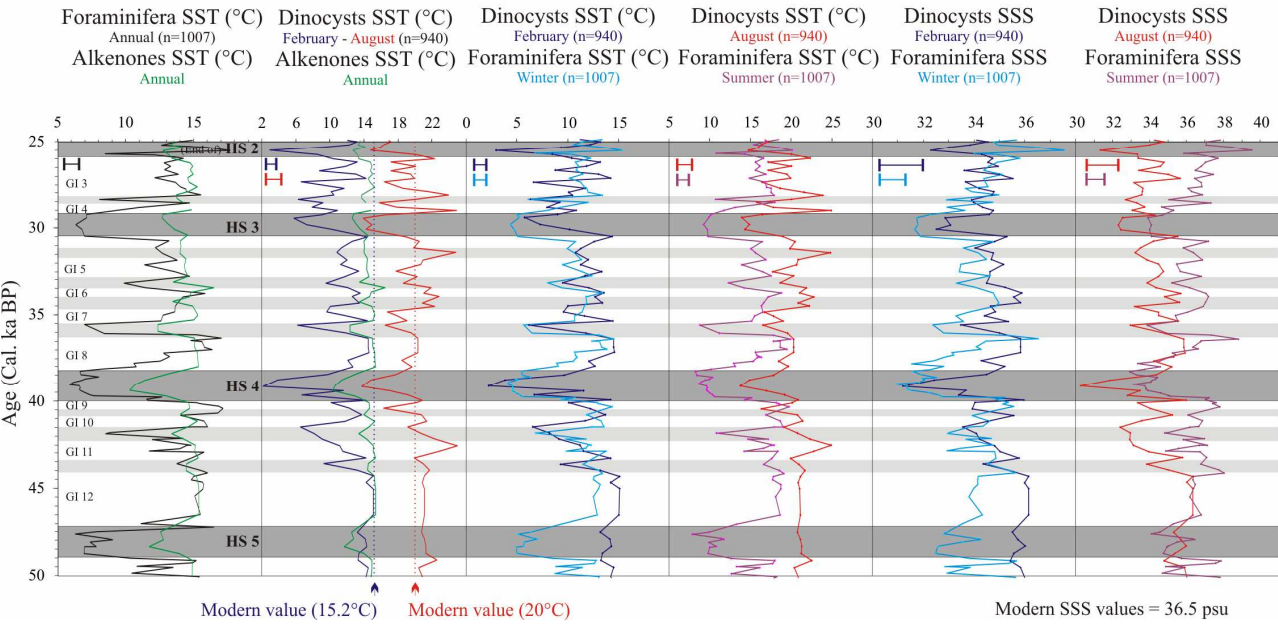


**Figure 2**

a) MD95-2043 - Alboran Sea



b) MD95-2042 - Iberian Margin



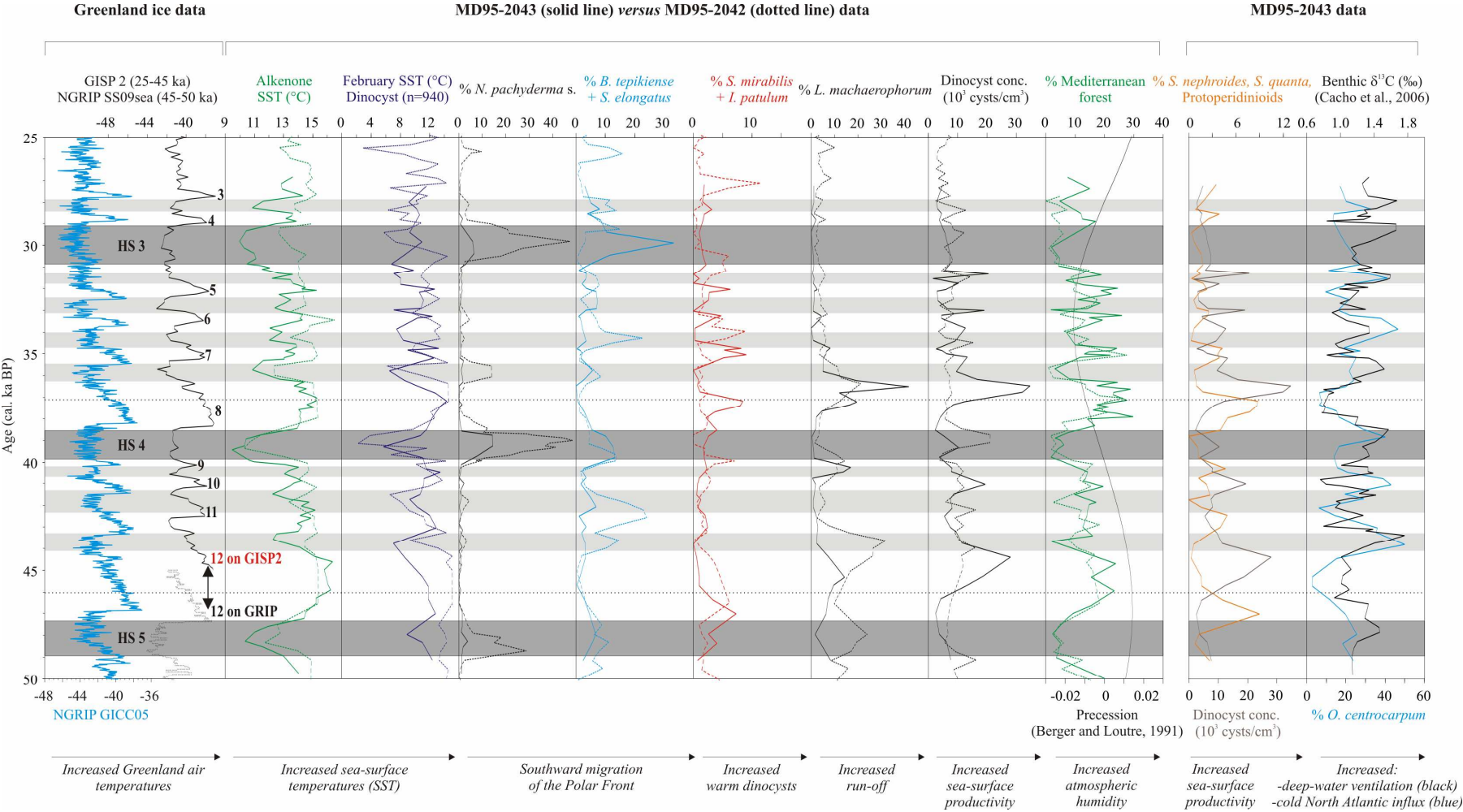
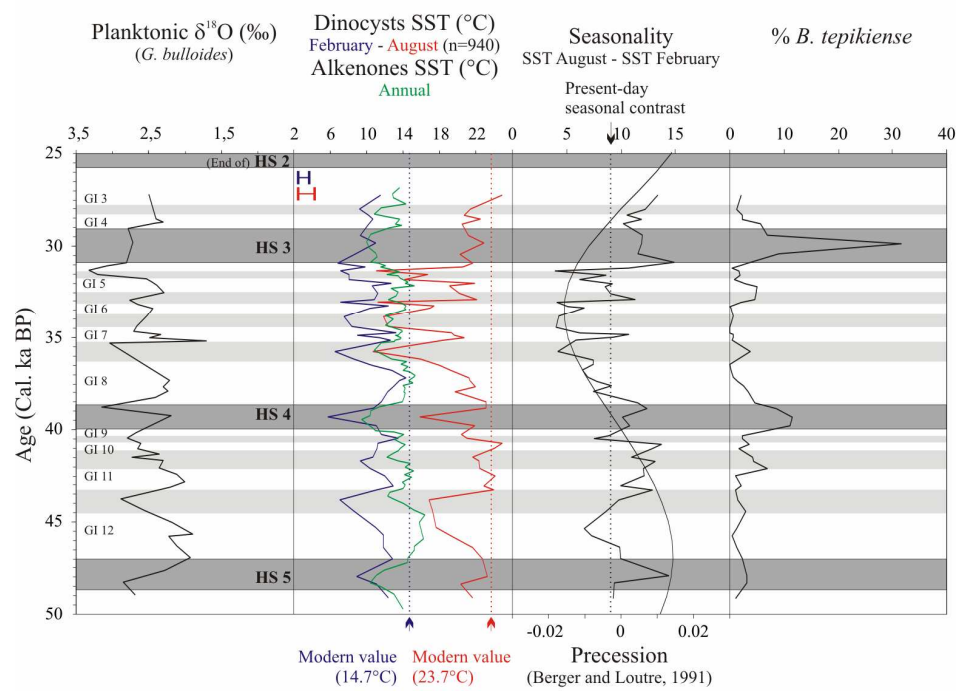


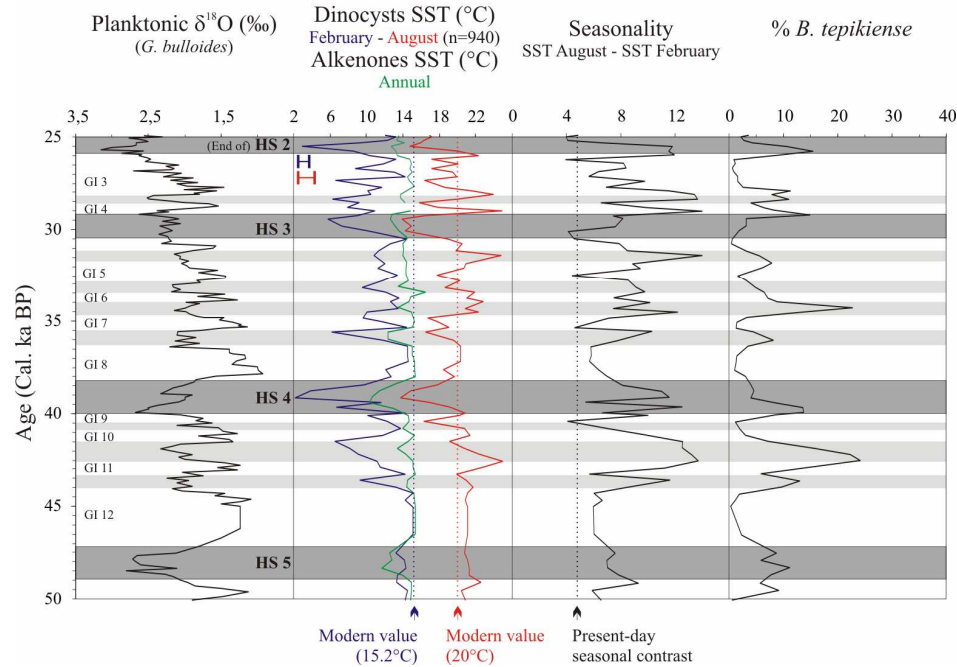
Figure 4



a) MD95-2043 - Alboran Sea



b) MD95-2042 - Iberian Margin



1579

1580 **Figure 5**

